Article

SARS-CoV-2 infection is effectively treated and prevented by EIDD-2801

https://doi.org/10.1038/s41586-021-03312-w

Received: 18 September 2020

Accepted: 29 January 2021

Published online: 9 February 2021

Check for updates

Angela Wahl[1,2,3,16], Lisa E. Gralinski[4,16], Claire E. Johnson[1,2,3], Wenbo Yao[1,2,3], Martina Kovarova[1,2,3], Kenneth H. Dinnon III[4,5], Hongwei Liu[6,7], Victoria J. Madden[8], Halina M. Krzystek[6,7], Chandrav De[1,2,3], Kristen K. White[8], Kendra Gully[4], Alexandra Schäfer[4], Tanzila Zaman[6,7], Sarah R. Leist[4], Paul O. Grant[6,7], Gregory R. Bluemling[9,10], Alexander A. Kolykhalov[9,10], Michael G. Natchus[10], Frederic B. Askin[11], George Painter[9,10,12], Edward P. Browne[2,3,5,13], Corbin D. Jones[6,7], Raymond J. Pickles[5,14], Ralph S. Baric[4,5,15] & J. Victor Garcia[1,2,3]✉

All coronaviruses known to have recently emerged as human pathogens probably originated in bats[1]. Here we use a single experimental platform based on immunodeficient mice implanted with human lung tissue (hereafter, human lung-only mice (LoM)) to demonstrate the efficient in vivo replication of severe acute respiratory syndrome coronavirus (SARS-CoV), Middle East respiratory syndrome coronavirus (MERS-CoV) and severe acute respiratory syndrome coronavirus 2 (SARS-CoV-2), as well as two endogenous SARS-like bat coronaviruses that show potential for emergence as human pathogens. Virus replication in this model occurs in bona fide human lung tissue and does not require any type of adaptation of the virus or the host. Our results indicate that bats contain endogenous coronaviruses that are capable of direct transmission to humans. Our detailed analysis of in vivo infection with SARS-CoV-2 in human lung tissue from LoM showed a predominant infection of human lung epithelial cells, including type-2 pneumocytes that are present in alveoli and ciliated airway cells. Acute infection with SARS-CoV-2 was highly cytopathic and induced a robust and sustained type-I interferon and inflammatory cytokine and chemokine response. Finally, we evaluated a therapeutic and pre-exposure prophylaxis strategy for SARS-CoV-2 infection. Our results show that therapeutic and prophylactic administration of EIDD-2801—an oral broad-spectrum antiviral agent that is currently in phase II/III clinical trials—markedly inhibited SARS-CoV-2 replication in vivo, and thus has considerable potential for the prevention and treatment of COVID-19.

SARS-CoV-2 has recently emerged in humans and is the causative agent of COVID-19; it has resulted in substantial morbidity and mortality worldwide[2]. Bats are the presumed source of SARS-CoV-2, as well as of the highly pathogenic human coronaviruses SARS-CoV and MERS-CoV[1]. Transmission of coronaviruses from bats to other species is well-documented and adaptation in an intermediary host can facilitate their transmission to humans[1]. Although it is possible that SARS-CoV-2 was transmitted to humans via an intermediate host, phylogenetic analysis has indicated that the SARS-CoV-2 lineage has circulated in bats for decades and that this virus has evolved in bats to be capable of replicating in human cells[3]. Given the repeated and accelerating emergence of highly pathogenic coronaviruses, it is increasingly important to monitor and characterize bat coronaviruses, and to identify the viral determinants of human infection, disease and global spread—as well as to develop effective therapeutic interventions. Animal models are useful for studying highly pathogenic human coronaviruses and the emergence potential of zoonotic coronaviruses, and for evaluating the in vivo inhibitory activity of novel agents[4–15]. However, human coronaviruses do not replicate in mice without extensive virus adaptation, genetic editing of the host receptor or the introduction of the appropriate human receptor genes into the host[4,6–13,15]. Although existing rodent models of coronavirus infection have made several important contributions, none possesses the diverse set of primary human lung cells that serve as targets for viral infection[16]. Here we show that immunodeficient mice implanted with authentic human lung tissue[17] (that is, LoM) allow for the in vivo study of infection with SARS-CoV, MERS-CoV or SARS-CoV-2 in a single platform that permits the direct comparison of experimental outcomes. Using

[1]International Center for the Advancement of Translational Science, University of North Carolina at Chapel Hill, Chapel Hill, NC, USA. [2]Division of Infectious Diseases, Department of Medicine, University of North Carolina at Chapel Hill, Chapel Hill, NC, USA. [3]Center for AIDS Research, University of North Carolina at Chapel Hill, Chapel Hill, NC, USA. [4]Department of Epidemiology, University of North Carolina at Chapel Hill, Chapel Hill, NC, USA. [5]Department of Microbiology and Immunology, University of North Carolina at Chapel Hill, Chapel Hill, NC, USA. [6]Department of Biology, University of North Carolina at Chapel Hill, Chapel Hill, NC, USA. [7]Department of Genetics, University of North Carolina at Chapel Hill, Chapel Hill, NC, USA. [8]Microscopy Services Laboratory, University of North Carolina at Chapel Hill, Chapel Hill, NC, USA. [9]Emory Institute of Drug Development (EIDD), Emory University, Atlanta, GA, USA. [10]Drug Innovation Ventures at Emory (DRIVE), Atlanta, GA, USA. [11]Department of Pathology, University of North Carolina at Chapel Hill, Chapel Hill, NC, USA. [12]Department of Pharmacology and Chemical Biology, Emory University, Atlanta, GA, USA. [13]UNC HIV Cure Center, University of North Carolina at Chapel Hill, Chapel Hill, NC, USA. [14]Marsico Lung Institute, University of North Carolina at Chapel, Chapel Hill, NC, USA. [15]Rapidly Emerging Antiviral Drug Discovery Initiative, University of North Carolina at Chapel Hill, Chapel Hill, NC, USA. [16]These authors contributed equally: Angela Wahl, Lisa E. Gralinski. ✉e-mail: victor_garcia@med.unc.edu

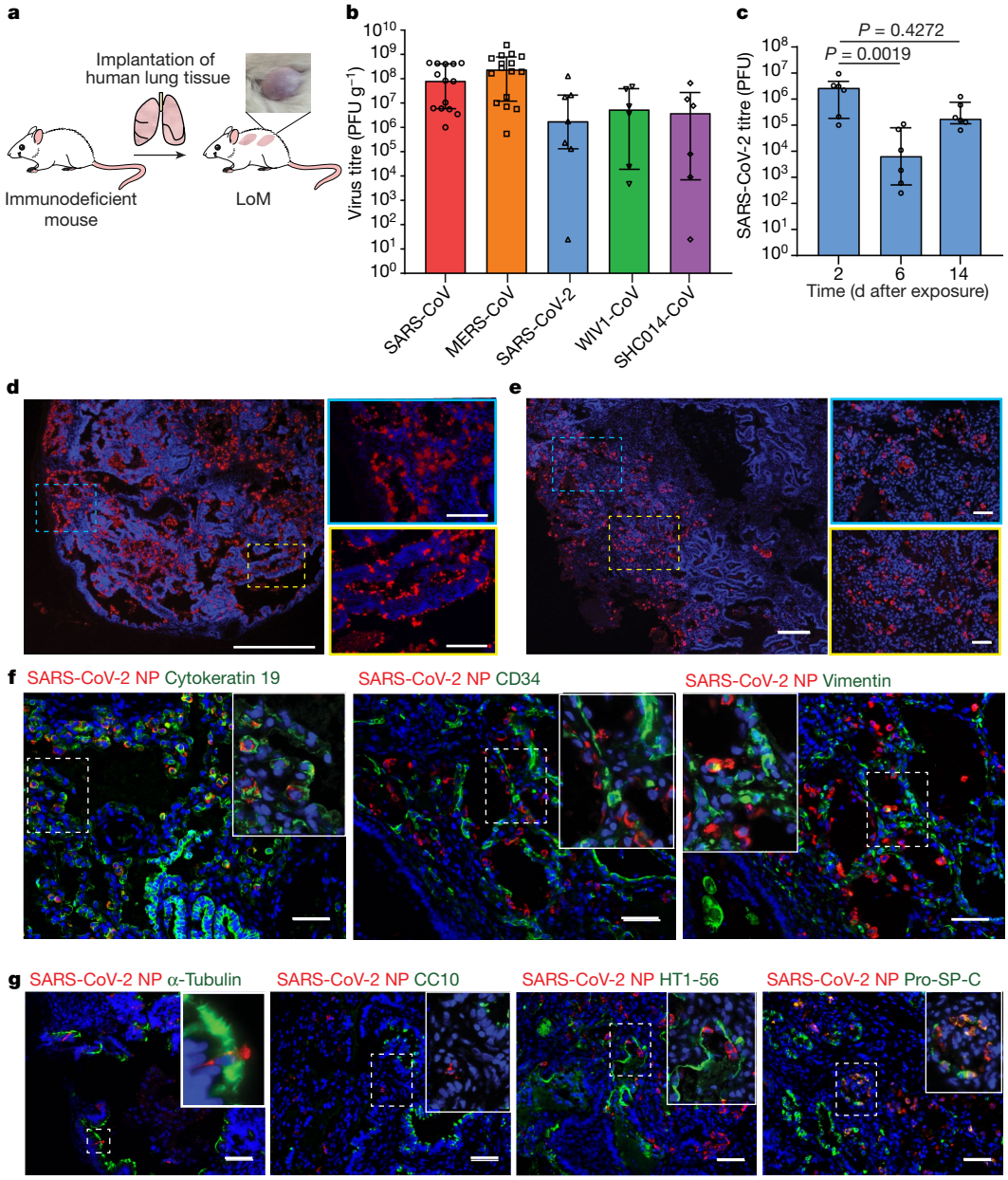

Fig. 1 | Robust replication of recently emerged human and bat coronaviruses in LoM and the predilection of SARS-CoV-2 for infection of human epithelial cells. a, LoM construction and image of a human lung implant. **b**, Viral titres in the human lung tissue of LoM injected with SARS-CoV ($n = 14$) (red), MERS-CoV ($n = 16$) (orange), SARS-CoV-2 ($n = 7$) (blue), WIV1-CoV ($n = 6$) (green) or SHC014 ($n = 6$) (purple), as determined by plaque assay. PFU, plaque-forming units. **c**, SARS-CoV-2 titres in the human lung tissue of LoM at days 2 ($n = 6$), 6 ($n = 6$) and 14 ($n = 6$) after exposure were compared with a two-sided Kruskal–Wallis with Dunn's multiple comparisons test. **d**, SARS-CoV-2 RNA in human lung tissue of LoM at two days after exposure. SARS-CoV-2 RNA-positive, red; nuclei, blue. Scale bars, 750 µm (left), 250 µm (top right, bottom right). $n = 3$. **e**, Virus nucleoprotein in human lung tissue of LoM two days after exposure. Nucleoprotein-positive cells, red; nuclei, blue. Scale bars, 200 µm (left), 50 µm (top right, bottom right). $n = 6$. **f**, Costaining of human lung tissue of LoM, two days after exposure to SARS-CoV-2, for virus nucleoprotein (NP) (red) and cytokeratin 19 (epithelial cells, green) ($n = 6$), CD34 (endothelial cells, green) ($n = 4$) or vimentin (mesenchymal cells, green) ($n = 4$). Nuclei, blue. Scale bars, 50 µm. **g**, Costaining of human lung tissue of LoM, two days after exposure to SARS-CoV-2, for virus nucleoprotein (red) and acetylated α-tubulin IV (ciliated cells, green) ($n = 6$), CC10 (club cells, green) ($n = 6$), HT1-56 (alveolar type-1 pneumocytes, green) ($n = 6$) or pro-SP-C (alveolar type-2 pneumocytes, green) ($n = 3$). Nuclei, blue. Scale bars, 50 µm. In **b**, **c**, horizontal and vertical lines represent the median and interquartile range, respectively. *n*, number of biologically independent lung tissues analysed.

LoM, we show efficient replication of bat coronaviruses in vivo without the need for virus adaptation. We also performed an in-depth in vivo analysis of acute SARS-CoV-2 infection in human lung tissue from LoM, which revealed robust virus replication, pathogenesis and sustained activation of the human innate immune response. Finally, we show that EIDD-2801—an orally administered, broad-spectrum antiviral agent that is currently in phase II/III clinical trials for the treatment of COVID-19—efficiently inhibited SARS-CoV-2 replication in human lung tissue from LoM when administered therapeutically, and prevented SARS-CoV-2 infection when administered as pre-exposure prophylaxis, which together strongly support its further clinical development for COVID-19.

Coronavirus replication in LoM

LoM are constructed by the subcutaneous implantation of human lung tissue into the back of immunodeficient mice (Fig. 1a). This tissue expands

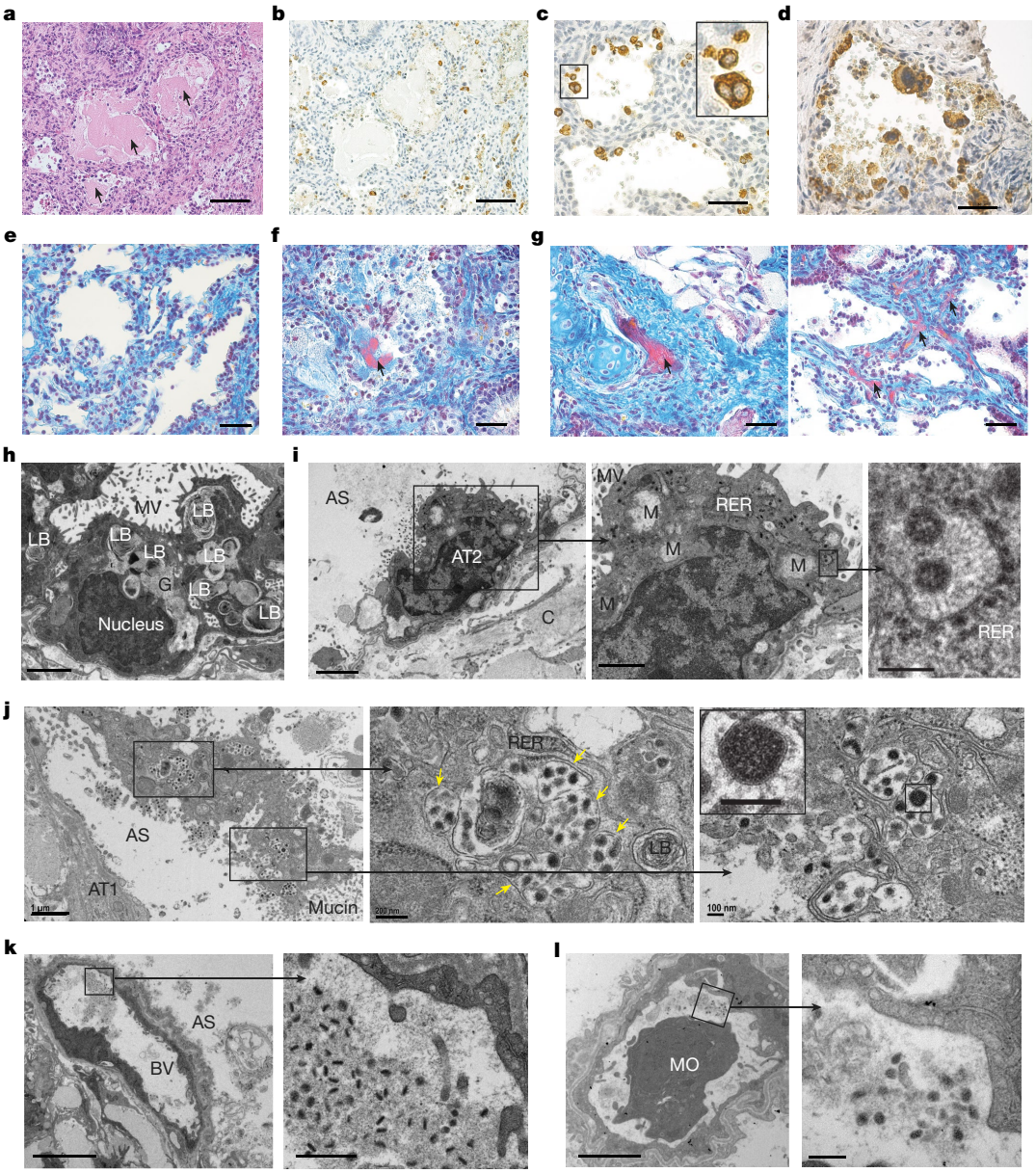

Fig. 2 | Acute SARS-CoV-2 infection is highly cytopathic and causes extensive damage to human lung structures. a, Haematoxylin and eosin (H&E) staining of human lung tissue from a SARS-CoV-2-infected LoM two days after exposure. $n = 6$. Scale bar, 100 µm. Arrows indicate protein globules. **b**–**d**, Immunohistochemical staining for virus nucleoprotein in human lung tissue of LoM two days after exposure to SARS-CoV-2. Nucleoprotein-positive cells, brown. Scale bars, 100 µm (**b**), 50 µm (**c**, **d**). $n = 6$. **e**–**g**, Martius Scarlet Blue staining of human lung tissue from naive LoM ($n = 6$) (**e**) and SARS-CoV-2 infected LoM two days after exposure ($n = 6$) (**f**, **g**). Fibrin, red; collagen, blue. Scale bars, 50 µm. Arrows indicate the presence of fibrin (red) in alveoli (**f**) or thrombi (**g**) of occluded vessels. **h**–**l**, Electron microscopy analysis of SARS-CoV-2-infected human lung tissue of LoM at two days after exposure ($n = 3$). **h**, Uninfected alveolar type-2 pneumocytes in an alveolus-like structure. Scale bar, 2 µm. **i**, SARS-CoV-2-infected alveolar type-2 pneumocyte. Higher-magnification images of boxed areas show virus particles with dense nucleocapsids in the rough endoplasmic reticulum. Scale bars, 2 µm (left), 1 µm (centre), 200 nm (right). **j**, Degenerative SARS-CoV-2-infected cell in the alveolar space. Arrows indicate virus-filled vesicles. Scale bars, 1 µm (left), 200 nm (centre), 100 nm (right). **k**, **l**, Blood vessels containing virions, fibrillar protein and cell debris. Scale bars, 5 µm (**k** left), 500 nm (**k** right), 2 µm (**l** right), 200 nm (**l** left). AS, alveolar space; AT1, alveolar type-1 pneumocytes; AT2, alveolar type-2 pneumocytes; BV, blood vessel; C, collagen; G, glycogen; LB, lamellar body; M, mitochondria; MO, monocyte; MV, microvilli; RER, rough endoplasmic reticulum. In **c**, **i**–**l**, black boxes indicate areas of higher magnification. *n*, number of biologically independent lung tissues analysed.

to form a palpable implant[17] (Fig. 1a). Lung implants contain human fibroblasts, epithelial, endothelial and mesenchymal cells that form cartilaginous and noncartilaginous bronchial airways that are lined with ciliated and nonciliated epithelium, alveolar sac structures and extensive vasculature[17] (Extended Data Fig. 1a, b). The human lung tissue in LoM has previously been shown to support the replication of a diverse set of emerging and clinically relevant human pathogens, including MERS-CoV[17].

We evaluated the potential of LoM to serve as a single platform to study all known recently emerged human coronaviruses and the potential of endogenous bat coronaviruses for human emergence. Human angiotensin-converting enzyme 2 (ACE2), which is the receptor used by SARS-CoV and SARS-CoV-2[18–21], is expressed on human epithelial cells (cytokeratin 19^{+}) in the human lung tissues of LoM (Extended Data Fig. 1c, d). We also confirmed the expression of transmembrane

protease serine 2 (TMPRSS2), which primes the spike protein of SARS-CoV and SARS-CoV-2[18], in these tissues (Extended Data Fig. 1e). We inoculated LoM with SARS-CoV, MERS-CoV or SARS-CoV-2 (Extended Data Table 1). Infection with SARS-CoV and SARS-CoV-2 resulted in mean virus titres of 1.76×10^8 and 2.42×10^7 plaque-forming units (PFU) g^{-1}, respectively, at 2 days after infection (Fig. 1b). We observed abundant viral nucleoprotein antigen in the human lung tissues of LoM infected with SARS-CoV or SARS-CoV-2 (Extended Data Fig. 2a). Consistent with previous results[17], MERS-CoV replicated to mean titres of 4.79×10^8 PFU g^{-1} in the human lung tissues of LoM at 2 days after infection (Fig. 1b), and we observed abundant viral nucleoprotein antigen (Extended Data Fig. 2a).

The bat coronaviruses WIV1-CoV and SHC014-CoV have high sequence homology to SARS-CoV, use ACE2 to infect human cells and grow modestly in primary human airway cultures on liquid interface[12,13]. WIV1-CoV and SHC014-CoV efficiently replicated in the human lung tissue of LoM (Extended Data Table 1), with mean titres of 1.58×10^7 and 1.48×10^7 PFU g^{-1}, respectively, at two days after exposure to the virus (Fig. 1b), and we readily detected viral nucleoprotein antigen in the human lung tissues (Extended Data Fig. 2b). We did not detect viral nucleoprotein antigen in the human lung tissues of naive LoM (Extended Data Fig. 2c). Collectively, these results demonstrate that LoM serve as a single platform in which the recently emerged human coronaviruses SARS-CoV, MERS-CoV and SARS-CoV-2 replicate efficiently in human lung tissue. Notably, the efficient replication of the SARS-like bat coronaviruses WIV1-CoV and SHC014-CoV that we observed is in agreement with previous in vitro data[12,13], suggesting that bats contain coronaviruses that are capable of direct transmission to humans—bypassing the need for further adaptation in an intermediary host.

SARS-CoV-2 replication in LoM

We inoculated the human lung tissues of LoM with SARS-CoV-2, and determined titres of replication-competent virus at 2, 6 and 14 days after exposure (Fig. 1c, Extended Data Table 2). We noted high titres of replication-competent virus at all of the time points we measured, although titres were highest at two days after infection (Fig. 1c). Infection was widely distributed throughout the tissue, and large numbers of cells were positive for viral RNA (Fig. 1d) and nucleoprotein (Fig. 1e). We costained for human cytokeratin 19, which demonstrated that SARS-CoV-2 predominantly infects human epithelial cells in the lung (Fig. 1f, Extended Data Fig. 3a). We did not detect viral nucleoprotein antigen in human CD34-expressing (endothelial) cells, and detected this antigen in only a few human vimentin-expressing (mesenchymal) cells (Fig. 1f, Extended Data Fig. 3a). We further identified the types of infected epithelial cell. We clearly identified virus nucleoprotein antigen in cells that express pro-SP-C (alveolar type-2 pneumocytes) or acetylated α-tubulin IV (ciliated cells), but not did not detect this antigen in HT1-56$^+$ cells (alveolar type-1 pneumocytes) or CC10$^+$ cells (club cells) (Fig. 1g, Extended Data Fig. 3b). These results demonstrate that SARS-CoV-2 has limited tropism in the lung, and that alveolar type-2 pneumocytes and ciliated airway epithelial cells are the predominant cells infected.

SARS-CoV-2 pathogenesis in LoM

Our histopathological analysis revealed several features of early diffuse alveolar damage that have previously been described in lung tissues of patients with COVID-19, including the accumulation of proteinaceous exudate and fibrin in alveolar spaces, desquamation of pneumocytes, multinucleated cell formation and the appearance of fibrin thrombi in small vessels[22–24] (Fig. 2). We observed proteinaceous exudate—including large protein globules—in alveolar spaces that overlapped with areas of virus accumulation (Fig. 2a, b). We noted desquamation of pneumocytes as early as two days after infection; a large number of virally infected cells were fully detached or detaching from the alveolar basement membrane (Fig. 2c, d). We also observed infected multinucleated cells (Fig. 2c). Although we did not note hyaline membranes, in contrast to naive LoM (Fig. 2e), we detected fibrin in alveolar spaces in human lung tissue from SARS-CoV-2-infected LoM (Fig. 2f). Notably, we observed several occluded vessels containing fibrin thrombi, as has previously been reported in the lungs of patients with COVID-19[22–24] (Fig. 2g). Our electron microscopy investigations demonstrated that the architecture and integrity of uninfected alveolar type-2 pneumocytes in human lung tissue obtained from LoM at two days after infection were normal (Fig. 2h). By contrast, alveolar type-2 pneumocytes (from the same sample) that contained virus particles had swollen mitochondria with a loss of matrix and cristae as well as rough endoplasmic reticula with distended cisternae, protein accumulation and virus particles (Fig. 2i). We observed degenerative alveolar type-2 pneumocytes infected with SARS-CoV-2 that were detached from the alveolar basal membrane in the alveolar luminal space (Fig. 2j). A higher magnification revealed the subcellular accumulation of virus-containing vesicles, indicative of virus replication and egress. We also observed virions with electron-dense nucleocapsids and distinctive crown-like spikes (Fig. 2i, j). Consistent with previous reports[23,25], the virions produced by human lung cells were pleomorphic in size (69 to 112 nm) and shape. Despite the extensive damage that we observed in the lung tissue, the endothelium in the majority of blood vessels was intact, and possessed tight junctions, numerous pinocytotic vesicles, and normal mitochondria and endoplasmic reticulum (Fig. 2k, l). We did not detect virions within endothelial cells, consistent with our immunofluorescence analysis (Figs. 1f, 2k, l). However, pleomorphic virions were present in capillary lumen and were surrounded by fibrillar protein deposits and cell debris (Fig. 2k, l). Together, these results demonstrate that acute SARS-CoV-2 infection of LoM closely resembles lung infection in humans, and that it is highly cytopathic (resulting in substantial injury to the fragile alveolar lung structures).

We performed RNA-sequencing analysis of human lung tissues collected from LoM at 2, 6 and 14 days after infection. We detected abundant viral transcripts that ranged from 0.55% to 3.6% of the total reads at 2 days after infection (Extended Data Table 3); viral transcripts were abundant but lower at 6 days and 14 days after infection (Extended Data Table 3). Our sequencing data identified canonical SARS-CoV-2 transcripts[26] and confirmed the maintenance of the furin cleavage site in the spike protein. Our analysis of human gene transcripts revealed 1,504 differentially expressed cellular genes between naive and infected human lung tissue from LoM at 2 days after exposure (the peak of infection) (Fig. 3a, Supplementary Tables 1, 2). Our differential expression analysis suggests that 1,043 of these genes were increased in expression, and 461 were decreased, in the infected human lung tissue of LoM relative to that of naive controls (Supplementary Tables 1, 2). We noted three patterns: the expression of most genes did not change with infection; many genes with increased expression in SARS-CoV-2-infected LoM were expressed at a low or moderate level in naive LoM; and a handful of genes went from undetectable expression in naive LoM to moderate or high expression in infected LoM, or from expression in naive LoM to undetectable expression in infected LoM. As expected, *ACE2* and *TMPRSS2* were expressed across the lung tissues (Extended Data Table 4). Notably, numerous interferon-stimulated genes and inflammatory cytokine genes—including the pro-inflammatory cytokine genes *IL6*, *CXCL8* (which encodes IL-8), *CXCL10* (which encodes IP-10), *TNF* and *CCL5* (which encodes RANTES)—were potently induced in infected human lung tissue from LoM (Supplementary Tables 1, 2). We also observed a marked upregulation of *IFNB1*, *IFNL1*, *IFNL2* and *IFNL3* expression (>1,000-fold for all) at 2 days after exposure, which suggests that these cytokines have a key role in the antiviral response to SARS-CoV-2 (Supplementary Tables 1, 2). Our gene set enrichment analysis showed that over 840 gene pathways were significantly upregulated ($P < 0.05$),

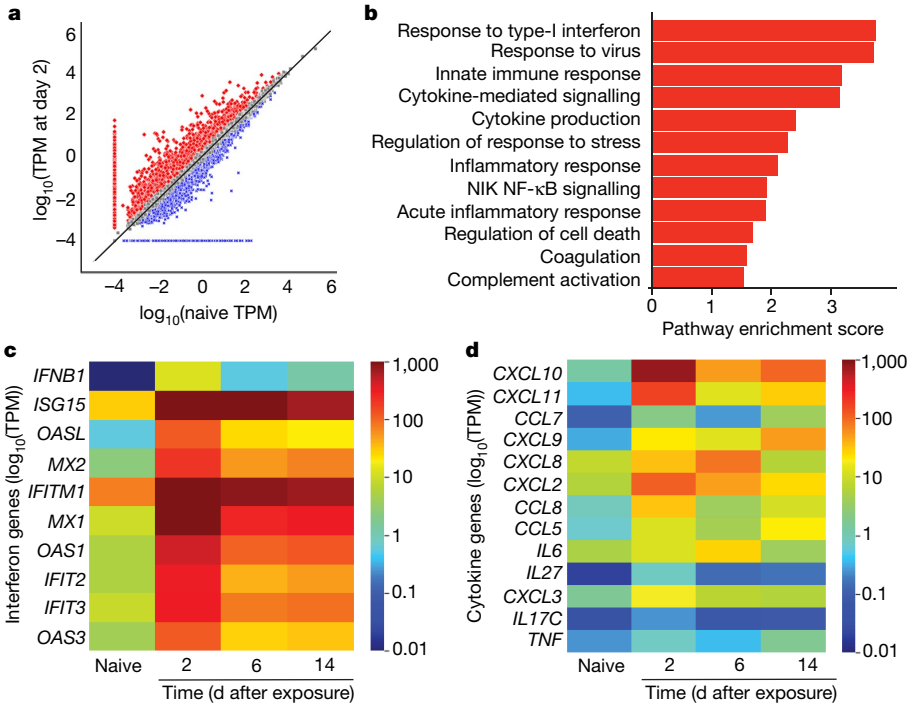

Fig. 3 | SARS-CoV-2 infection induces a strong and sustained human innate immune response in human lung tissue from LoM. a–**d**, RNA-sequencing analysis of human lung tissue collected from SARS-CoV-2-infected LoM. **a**, $\log_{10}$-transformed gene transcripts per million (TPM) in the human lungs of naive LoM ($n = 2$) (*x* axis) and SARS-CoV-2-infected LoM on day 2 after exposure ($n = 2$) (*y* axis). Genes of interest from Supplementary Tables 1, 2 that appear increased (red) or decreased (blue) by at least twofold in SARS-CoV-2-infected LoM are shown. Genes with zero (0) mean TPM in naive or infected LoM are set at a minimum of $\log_{10}(0.0001)$ TPM for visualization. **b**, Gene set enrichment analysis identified gene sets enriched in human lung tissue from SARS-CoV-2-infected LoM. The pathway enrichment score is shown on the *x* axis. The statistical significance of enrichment scores was determined using a two-sided empirical phenotype-based permutation test, and adjusted for multiple testing using a false discovery rate (red, $P < 0.05$). **c**, **d**, Heat maps illustrating the expression of human interferon genes (**c**) and cytokine and chemokine genes (**d**) in human lung tissue collected from SARS-CoV-2-infected LoM on days 2 ($n = 2$), 6 ($n = 3$) and 14 ($n = 3$) after exposure, and from naive LoM ($n = 4$). Colour scale indicates the mean $\log_{10}$(TPM). *n*, number of biologically independent lung tissues analysed.

including response to type-I interferon ($P = 0.0011$), response to virus ($P = 0.0010$), innate immune response ($P = 0.0010$), cytokine-mediated signalling ($P = 0.0010$), cytokine production ($P = 0.0010$), response to stress ($P = 0.0010$), inflammatory response ($P = 0.0010$), NIK NF-κB signalling ($P = 0.0011$), acute inflammatory response ($P = 0.0035$), regulation of cell death ($P = 0.0030$) and coagulation pathways ($P = 0.0453$) (Fig. 3b). Complement activation, which contributes to SARS-CoV pathogenesis in mouse models[14], was also increased ($P = 0.0470$) (Fig. 3b). Importantly, our analysis of host gene expression at later time points demonstrated a sustained upregulation of antiviral and inflammatory genes that—in some instances (for example, *ISG15*, *IFITM1*, *TNF* and *CXCL9*)—persisted for up to 14 days after infection (the final time point that we analysed) (Fig. 3c, d, Extended Data Table 5, Supplementary Tables 1, 2). These results demonstrate that acute SARS-CoV-2 infection causes a potent and sustained upregulation of innate immune responses in virus-infected human lung tissue of LoM.

EIDD-2801 treatment and prophylaxis

The ribonucleoside analogue β-D-N^4-hydroxycytidine (NHC) broadly inhibits coronavirus infection in vitro in cultures of human airway epithelial cells[15]. Prophylactic and therapeutic administration of the oral pro-drug of NHC (EIDD-2801; also known as molnupiravir or MK-4482) reduced SARS-CoV and MERS-CoV replication and pathogenesis in mice[15]. 5′-triphosphate NHC acts as a competitive alternate substrate for the viral RNA-dependent RNA polymerase, which allows the incorporation of 5′-triphosphate NHC into viral RNA and results in the accumulation of mutations within the viral RNA genome that lead to error catastrophe[15]. As an orally bioavailable agent, EIDD-2801 can be administered to patients much more readily than can remdesivir and other antiviral and biological agents (for example, convalescent plasma and monoclonal antibodies), which require administration by infusion in a clinical setting. We tested the ability of therapeutic use of EIDD-2801 to inhibit SARS-CoV-2 replication in vivo in LoM, using a dose that is similar to the human dose in clinical trials[27]. We administered EIDD-2801 to LoM starting at 24 or 48 h after exposure to SARS-CoV-2, and every 12 h thereafter (Extended Data Fig. 4a, Extended Data Table 6). Our results show that EIDD-2801 had a notable effect on virus replication after only two days of treatment (Fig. 4a, b). EIDD-2801 markedly reduced the number of infectious particles in the human lung tissue of LoM by 4.4 logs (>25,000-fold decrease) when treatment was initiated at 24 h after exposure ($P = 0.0002$) (Fig. 4a). When treatment was started at 48 h after exposure, virus titres were significantly reduced by 96% (1.5 logs, $P = 0.0019$) (Fig. 4b). Next, we tested the efficacy of pre-exposure prophylaxis using EIDD-2801. We administered EIDD-2801 to LoM starting 12 h before exposure to SARS-CoV-2, and every 12 h thereafter (Extended Data Fig. 4b, Extended Data Table 6). EIDD-2801 pre-exposure prophylaxis significantly reduced virus titres in the human lung tissues of LoM by over 100,000-fold in 2 independent experiments ($P = 0.0002$ and $P = 0.0068$) (Fig. 4c–e). Furthermore, in contrast to the situation in mice treated with EIDD-2801, we observed abundant cell debris and nucleoprotein-positive cells in the alveolar lumen of mice treated with vehicle control, consistent with the extensive pathogenic effects inflicted on the lung by SARS-CoV-2 (Fig. 4f, g).

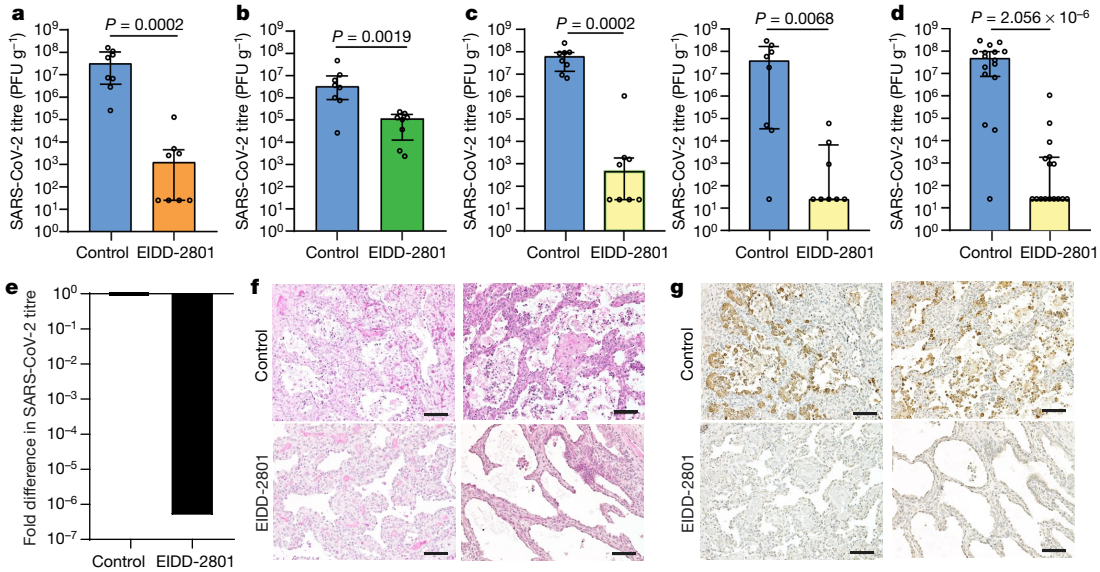

Fig. 4 | Treatment and pre-exposure prophylaxis with EIDD-2801 potently inhibit SARS-CoV-2 infection in vivo. a, SARS-CoV-2 titres in the human lung tissue of LoM administered EIDD-2801 ($n = 8$) or vehicle control ($n = 8$) 24 h after exposure to virus. **b**, SARS-CoV-2 titres in the human lung tissue of LoM administered EIDD-2801 ($n = 8$) or vehicle ($n = 8$) 48 h after exposure to virus. **c**, **d**, SARS-CoV-2 titres in the human lung tissue of LoM administered EIDD-2801 ($n = 8$ per experiment) or control vehicle ($n = 8$ per experiment) 12 h before exposure to virus in two independent experiments shown separately (**c**) and combined (**d**). **e**, Fold difference in SARS-CoV-2 titres in the human lung tissue of LoM administered EIDD-2801 12 h before exposure to virus relative to vehicle controls. **f**, **g**, H&E staining (**f**) and immunohistochemical staining (**g**) for virus nucleoprotein (nucleoprotein-positive cells, brown) of human lung tissue of LoM administered EIDD-2801 ($n = 8$) or control vehicle ($n = 8$) 12 h before exposure to virus. Scale bars, 100 µm. **a**–**d**, Titres were compared with a two-tailed Mann–Whitney *U* test. Horizontal and vertical lines represent the median and interquartile range, respectively. *n*, number of biologically independent lung tissues analysed.

These results demonstrate that prophylactic administration of EIDD-2801 is highly effective at preventing SARS-CoV-2 infection and pathogenesis in vivo in the human lung tissues of LoM.

Discussion

Our results demonstrate replication of all known recently emerged human coronaviruses in LoM. Importantly, consistent with in vitro studies[12,13], our results demonstrate the relatively efficient replication of two endogenous bat viruses in the human lung tissue of LoM in vivo, which indicates that coronaviruses circulating in bats have pandemic potential without the need for further adaptation to humans. Acute SARS-CoV-2 infection of LoM resulted in substantial lung injury and exhibited key features of the extensive lung pathology observed in patients with severe COVID-19[22,24,28,29]. Consistent with analyses of bronchoalveolar fluid or post-mortem lung samples obtained from patients with COVID-19[5,30], several interferon-stimulated genes were significantly increased in SARS-CoV-2-infected human lung tissue from LoM. We observed a robust induction of *IFNB1* expression during acute infection, followed by a decline in expression. A post-mortem analysis of the lungs of patients with COVID-19[5] did not reveal increased *IFNB1* expression, and it has previously been shown in vitro that the expression of *IFNB1* is blocked during SARS-CoV infection[31,32]. These results suggest that, in human lung tissue, *IFNB1* expression is induced during acute SARS-CoV-2 infection. Although this study was not designed to evaluate the effect of type-I interferon on SARS-CoV-2 replication in vivo, in vitro studies and in vivo mouse studies have shown that treatment with type-I interferon restricts SARS-CoV-2 replication[7,33]. We also observed an increased expression of several human cytokine genes in SARS-CoV-2-infected LoM, many of which have also been shown to be increased in analyses of serum and post-mortem lung tissue from patients with COVID-19—further establishing the similarities between LoM and human SARS-CoV-2 infection[5,34].

The SARS-CoV-2 vaccines that have been authorized for emergency use by the US Food and Drug Administration are highly effective at preventing disease. However, it may take considerable time to reach the target vaccination levels that are needed for herd immunity (especially in resource-limited settings), owing to manufacturing capabilities, required vaccine shipping and storage conditions, and public acceptance. Therefore, alternative treatments and preventive approaches are still urgently needed. Remdesivir is limited to use in hospitalized patients, and its effectiveness at reducing disease and mortality late in infection is not clear[35,36]. Although a carefully controlled clinical trial sponsored by the National Institutes of Health has reported that remdesivir significantly shortened the time of recovery[35], the SOLIDARITY trial of the World Health Organization revealed no significant reduction in the duration of hospitalization or mortality[36]. The early administration of the monoclonal antibody therapies bamlanivimab and REGN-CoV2 significantly reduced viral loads in patients with COVID-19 who exhibited mild-to-moderate disease[37,38]. However, these agents must be administered by infusion in a clinical setting, which limits their potential for widespread use. A highly efficacious antiviral agent that is administered orally has the potential for more widespread use, and for administration to patients with mild-to-moderate disease[39]. Here we show that EIDD-2801 administered therapeutically to LoM for only two days significantly reduced infectious virus titres in vivo by over 4 logs; the sooner that the EIDD-2801 treatment was initiated after exposure to SARS-CoV-2 exposure, the greater was the reduction in virus replication. We also observed that prophylactic administration of EIDD-2801 efficiently prevents SARS-CoV-2 infection in vivo, which highlights the potential utility of EIDD-2801 as an effective prophylactic and therapeutic agent against SARS-CoV-2 (as well as, potentially, other past and future zoonotic coronaviruses). NHC belongs to a class of ribonucleoside analogues that are known to often affect mitochondrial replication and function. However, NHC did not cause significant mitochondrial toxicity or impair mitochondrial function in vitro[40]. Furthermore, no significant increase

in transition frequencies in nuclear or mitochondrial message was detected in the lung tissue of ferrets dosed with EIDD-2801 for seven days, consistent with the observed good tolerability of the drug[41]. In ferrets, therapeutic administration of EIDD-2801 led to a reduction in SARS-CoV-2 titres in nasal passages and prevented transmission to co-housed naive animals[42]. Phase II and phase II/III clinical trials are ongoing to evaluate the safety of EIDD-2801 and its effect on viral shedding using doses up to 1,600 mg per day, a dose that is expected to provide similar intracellular levels of 5′-triphosphate NHC to those of a dose of 300–500 mg per kg body weight in mice. As with any antiviral agent, the therapeutic and prophylactic use of EIDD-2801 will be dictated by risk–benefit analyses. The limitations of our study include the absence of human nasal airway structures in LoM; these are thought to be early sites of SARS-CoV-2 replication in humans[43]. Because LoM do not have an autologous human adaptive immune system, they reflect the direct effect of viruses on their targets and bystander cells as well as the innate immune response to infection. Collectively, our results demonstrate the utility of LoM as a single in vivo platform to evaluate and compare the replication and pathogenesis of past, present and future pre-emergent, epidemic and pandemic coronaviruses, which will allow for accelerating the development and testing of therapeutic and pre-exposure prophylaxis agents such as EIDD-2801.

Online content

Any methods, additional references, Nature Research reporting summaries, source data, extended data, supplementary information, acknowledgements, peer review information; details of author contributions and competing interests; and statements of data and code availability are available at https://doi.org/10.1038/s41586-021-03312-w.

1. Cui, J., Li, F. & Shi, Z. L. Origin and evolution of pathogenic coronaviruses. *Nat. Rev. Microbiol.* **17**, 181–192 (2019).
2. Dong, E., Du, H. & Gardner, L. An interactive web-based dashboard to track COVID-19 in real time. *Lancet Infect. Dis.* **20**, 533–534 (2020).
3. Boni, M. F. et al. Evolutionary origins of the SARS-CoV-2 sarbecovirus lineage responsible for the COVID-19 pandemic. *Nat. Microbiol.* **5**, 1408–1417 (2020).
4. Bao, L. et al. The pathogenicity of SARS-CoV-2 in hACE2 transgenic mice. *Nature* **583**, 830–833 (2020).
5. Blanco-Melo, D. et al. Imbalanced host response to SARS-CoV-2 drives development of COVID-19. *Cell* **181**, 1036–1045 (2020).
6. Cockrell, A. S. et al. A mouse model for MERS coronavirus-induced acute respiratory distress syndrome. *Nat. Microbiol.* **2**, 16226 (2017).
7. Dinnon, K. H. III et al. A mouse-adapted model of SARS-CoV-2 to test COVID-19 countermeasures. *Nature* **586**, 560–566 (2020).
8. Gralinski, L. E. et al. Complement activation contributes to severe acute respiratory syndrome coronavirus pathogenesis. *MBio* **9**, e01753-18 (2018).
9. Jiang, R. D. et al. Pathogenesis of SARS-CoV-2 in transgenic mice expressing human angiotensin-converting enzyme 2. *Cell* **182**, 50–58.e8 (2020).
10. McCray, P. B. Jr et al. Lethal infection of K18-hACE2 mice infected with severe acute respiratory syndrome coronavirus. *J. Virol.* **81**, 813–821 (2007).
11. Menachery, V. D. et al. Middle East respiratory syndrome coronavirus nonstructural protein 16 is necessary for interferon resistance and viral pathogenesis. *MSphere* **2**, e00346-17 (2017).
12. Menachery, V. D. et al. A SARS-like cluster of circulating bat coronaviruses shows potential for human emergence. *Nat. Med.* **21**, 1508–1513 (2015).
13. Menachery, V. D. et al. SARS-like WIV1-CoV poised for human emergence. *Proc. Natl Acad. Sci. USA* **113**, 3048–3053 (2016).
14. Rockx, B. et al. Comparative pathogenesis of COVID-19, MERS, and SARS in a nonhuman primate model. *Science* **368**, 1012–1015 (2020).
15. Sheahan, T. P. et al. An orally bioavailable broad-spectrum antiviral inhibits SARS-CoV-2 in human airway epithelial cell cultures and multiple coronaviruses in mice. *Sci. Transl. Med.* **12**, eabb5883 (2020).
16. Franks, T. J. et al. Resident cellular components of the human lung: current knowledge and goals for research on cell phenotyping and function. *Proc. Am. Thorac. Soc.* **5**, 763–766 (2008).
17. Wahl, A. et al. Precision mouse models with expanded tropism for human pathogens. *Nat. Biotechnol.* **37**, 1163–1173 (2019).
18. Hoffmann, M. et al. SARS-CoV-2 cell entry depends on ACE2 and TMPRSS2 and is blocked by a clinically proven protease inhibitor. *Cell* **181**, 271–280 (2020).
19. Li, W. et al. Angiotensin-converting enzyme 2 is a functional receptor for the SARS coronavirus. *Nature* **426**, 450–454 (2003).
20. Walls, A. C. et al. Structure, function, and antigenicity of the SARS-CoV-2 spike glycoprotein. *Cell* **181**, 281–292 (2020).
21. Yan, R. et al. Structural basis for the recognition of SARS-CoV-2 by full-length human ACE2. *Science* **367**, 1444–1448 (2020).
22. Carsana, L. et al. Pulmonary post-mortem findings in a series of COVID-19 cases from northern Italy: a two-centre descriptive study. *Lancet Infect. Dis.* **20**, 1135–1140 (2020).
23. Menter, T. et al. Postmortem examination of COVID-19 patients reveals diffuse alveolar damage with severe capillary congestion and variegated findings in lungs and other organs suggesting vascular dysfunction. *Histopathology* **77**, 198–209 (2020).
24. Tian, S. et al. Pulmonary pathology of early-phase 2019 novel coronavirus (COVID-19) pneumonia in two patients with lung cancer. *J. Thorac. Oncol.* **15**, 700–704 (2020).
25. Zhu, N. et al. A novel coronavirus from patients with pneumonia in China, 2019. *N. Engl. J. Med.* **382**, 727–733 (2020).
26. Kim, D. et al. The architecture of SARS-CoV-2 transcriptome. *Cell* **181**, 914–921 (2020).
27. Merck Sharp & Dohme Corp. *Efficacy and Safety of Molnupiravir (MK-4482) in Hospitalized Adult Participants With COVID-19 (MK-4482–001)*, https://ClinicalTrials.gov/show/NCT04575584 (2020).
28. Xu, Z. et al. Pathological findings of COVID-19 associated with acute respiratory distress syndrome. *Lancet Respir. Med.* **8**, 420–422 (2020).
29. Zhang, H. et al. Histopathologic changes and SARS-CoV-2 immunostaining in the lung of a patient with COVID-19. *Ann. Intern. Med.* **172**, 629–632 (2020).
30. Zhou, Z. et al. Heightened innate immune responses in the respiratory tract of COVID-19 patients. *Cell Host Microbe* **27**, 883–890 (2020).
31. Siu, K. L. et al. Severe acute respiratory syndrome coronavirus M protein inhibits type I interferon production by impeding the formation of TRAF3.TANK.TBK1/IKKε complex. *J. Biol. Chem.* **284**, 16202–16209 (2009).
32. Spiegel, M. et al. Inhibition of beta interferon induction by severe acute respiratory syndrome coronavirus suggests a two-step model for activation of interferon regulatory factor 3. *J. Virol.* **79**, 2079–2086 (2005).
33. Vanderheiden, A. et al. Type I and type III interferons restrict SARS-CoV-2 infection of human airway epithelial cultures. *J. Virol.* **94**, e00985-20 (2020).
34. Qin, C. et al. Dysregulation of immune response in patients with coronavirus 2019 (COVID-19) in Wuhan, China. *Clin. Infect. Dis.* **71**, 762–768 (2020).
35. Beigel, J. H. et al. Remdesivir for the treatment of Covid-19 – final report. *N. Engl. J. Med.* **383**, 1813–1826 (2020).
36. WHO Solidarity Trial Consortium. Repurposed antiviral drugs for COVID-19 –interim WHO Solidarity trial results. *N. Engl. J. Med.* **384**, 497–511 (2021).
37. Chen, P. et al. SARS-CoV-2 neutralizing antibody LY-CoV555 in outpatients with Covid-19. *N. Engl. J. Med.* **384**, 229–237 (2021).
38. Regeneron Pharmaceuticals Inc. Regeneron's COVID-19 outpatient trial prospectively demonstrates that REGN-COV2 antibody cocktail significantly reduced virus levels and need for further medical attention. https://newsroom.regeneron.com/news-releases/news-release-details/regenerons-covid-19-outpatient-trial-prospectively-demonstrates (2020).
39. Kim, P. S., Read, S. W. & Fauci, A. S. Therapy for early COVID-19: a critical need. *J. Am. Med. Assoc.* **324**, 2149–2150 (2020).
40. Sticher, Z. M. et al. Analysis of the potential for N^4-hydroxycytidine to inhibit mitochondrial replication and function. *Antimicrob. Agents Chemother.* **64**, e01719-19 (2020).
41. Toots, M. et al. Characterization of orally efficacious influenza drug with high resistance barrier in ferrets and human airway epithelia. *Sci. Transl. Med.* **11**, eaax5866 (2019).
42. Cox, R. M., Wolf, J. D. & Plemper, R. K. Therapeutically administered ribonucleoside analogue MK-4482/EIDD-2801 blocks SARS-Cov-2 transmission in ferrets. *Nat. Microbiol.* **6**, 11–18 (2021).
43. Hou, Y. J. et al. SARS-CoV-2 reverse genetics reveals a variable infection gradient in the respiratory tract. *Cell* **182**, 429–446 (2020).

Methods

No statistical methods were used to predetermine sample size. The experiments were not randomized, and investigators were not blinded to allocation during experiments and outcome assessment.

Ethics statement

Mouse studies were carried out according to protocols approved by the Institutional Use and Care Committee at UNC Chapel Hill and in adherence to the NIH Guide for the Care and Use of Laboratory Animals. Mice were kept on a 12-h light/12-h dark cycle and housed in a temperature (20-23 °C)- and humidity (30–70%)-controlled vivarium maintained by the Division of Comparative Medicine at the University of North Carolina Chapel Hill.

Experimental design

LoM were used as an in vivo model to evaluate the infection of lung tissue with the recombinant coronaviruses SARS-CoV, MERS-CoV and SARS-CoV-2, as well as the full-length bat coronaviruses WIV1-CoV and SHC014-CoV[12,13,44,45]. Viruses were directly injected into the human lung tissue of LoM, and lung tissue was collected 2, 6 or 14 days after exposure to determine virus titre and/or for analysis by histology, electron microscopy or RNA sequencing.

Construction of humanized mice

LoM were constructed with 1 or 2 human lung implants by surgically implanting human lung tissue (Advanced Bioscience Resources) subcutaneously into the upper and lower back of male and female 12–21-week- old *NOD.Cg-Prkdc*^{scid} *Il2rg*^{tm1Wjl}*/SzJ* mice (NSG mice) (The Jackson Laboratory), as previously described[17]. Engraftment of lung tissue was assessed by palpation, and by eight weeks after surgery mice were ready for experimentation.

Production of coronavirus stocks and infection of humanized mice

Stocks of wild-type SARS-CoV, MERS-CoV (HCoV-EMC/2012), SHC014-CoV and WIV1-CoV were derived from infectious virus clones and were prepared and titred on Vero E6 (SARS-CoV, SHC014-CoV and WIV1-CoV) or Vero CCL81 cells (MERS-CoV) (American Type Culture Collection), as previously described[6,12,13,17]. Cell lines were authenticated by morphological identification and virus susceptibility profiles, and tested for mycoplasma by the supplier. A clinical isolate of SARS-CoV-2 (2019-nCoV/USA-WA1/2020) was obtained from the US Centers for Disease Control and Prevention (GenBank accession number MN985325.1) and passaged twice in Vero E6 cells to create a passage-5 working stock[43]. For the infection of mice with coronavirus, the fur over the human lung tissue of the anaesthetized LoM was shaved and virus ($1–3 \times 10^5$ PFU in 100 µl PBS) was injected directly into the lung tissue. To evaluate the in vivo inhibitory activity of pre-exposure prophylaxis using EIDD-2801, mice were administered 500 mg kg^{-1} EIDD-2801 or vehicle control (10% PEG and 2.5% Cremophor RH40 in water) via oral gavage starting 12 h before exposure to SARS-CoV-2, and every 12 h thereafter. The therapeutic efficacy of EIDD-2801 was assessed by administering mice 500 mg kg^{-1} EIDD-2801 or vehicle control (10% PEG and 2.5% Cremophor RH40 in water) via oral gavage starting 24 h or 48 h after exposure, and every 12 h thereafter. At necropsy, human lung tissues of LoM were collected, weighed (mean weight of 0.55 ± 0.05 g (±s.e.m.); $n = 32$), homogenized, and stored at −80 °C until titring on Vero E6 cells. Titres below the limit of the assay (50 PFU ml^{-1}) were assigned a value of 25 PFU g^{-1}. No correlation was observed between SARS-CoV-2 titre (PFU g^{-1}) at 2 days after exposure and the timing after surgery ($P = 0.4474$, two-tailed Spearman's rank correlation).

H&E staining of human lung tissue from LoM

Human lung tissues collected from LoM were fixed in 10% formalin, paraffin-embedded and cut into 5-µm sections, which were mounted onto Superfrost Plus slides (Fisher Scientific). Tissue sections were incubated at 60 °C for 1 h, deparaffinized with xylene (2× 3 min) and graded ethanol (100% 2× 3 min, 95% 1× 3 min, 80% 1× 3 min, 70% 1× 3 min), and stained with haematoxylin followed by eosin. Tissue sections were then mounted and imaged on a Nikon Eclipse Ci microscope using Nikon Elements BR software (version 4.30.01) with a Nikon Digital Sight DS-Fi2 camera. Brightness, contrast and white balance were adjusted on whole images in Adobe Photoshop (CS6).

Immunohistochemical analysis of coronavirus infection

Immunohistochemistry was performed as previously described[17]. In brief, fixed (10% formalin) human lung tissues collected from coronavirus-infected LoM were paraffin-embedded and sectioned (5 µm). Tissue sections mounted on Superfrost Plus slides (Fisher Scientific) were deparaffinized as described in 'H&E staining of human lung tissue from LoM'. Following antigen retrieval using Diva Decloaker (BioCare Medical), nonspecific binding was blocked using Background Sniper (BioCare Medical). Tissue sections were then incubated with primary antibodies against SARS-CoV nucleocapsid (1:500 or 1:1,000), MERS-CoV nucleocapsid (1:2,000) or TMPRSS2 (1:100) overnight at 4 °C. Tissue sections incubated with rabbit IgG were used as isotype controls. Tissue sections were then washed in TBST and the endogenous peroxidase activity was blocked with hydrogen peroxide. Tissue sections were developed using the MACH-3 polymer system (BioCare Medical) and 3,3′-diaminobenzidine (DAB) (Vector Laboratories), counterstained with haematoxylin and mounted. Tissue sections were imaged on a Nikon Eclipse Ci microscope using Nikon Elements BR software (version 4.30.01) with a Nikon Digital Sight DS-Fi2 camera. Adobe Photoshop (CS6) was used to adjust brightness, contrast and white balance on whole images.

Immunofluorescence analysis of SARS-CoV-2 infection

Human lung tissues collected from LoM were fixed in 10% formalin and paraffin-embedded. Immunofluoresence staining of 5-µm tissue sections was performed as previously described[17]. In brief, following deparaffinization and antigen retrieval (Diva Decloaker), tissue sections were incubated with a 10% normal donkey serum solution with 0.1% Triton X-100 in 1× PBS to block nonspecific binding. Tissue sections were then incubated overnight with primary antibodies at 4 °C, followed by incubation with fluorescent conjugated secondary antibodies. Primary antibodies were directed against SARS-CoV-2 nucleoprotein (1:500 or 1:1,000), ACE2 (1:200), human cytokeratin 19 (1:250), CD34 (1:100), vimentin (1:100), acetylated α-tubulin IV, CC10 (1:500), HT1-56 (1:150) and pro-SP-C (1:500). Secondary antibodies were: donkey anti-mouse IgG heavy and light chains–AlexaFluor 488 (1:1,000), donkey anti-rabbit IgG heavy and light chains–AlexaFluor 488(1:1,000), donkey anti-goat IgG heavy and light chains–AlexaFluor 594 (1:1,000), donkey anti-mouse IgG heavy and light chains–AlexaFluor Plus 594 (1:1,000), donkey anti-rabbit IgG heavy and light chains–AlexaFluor Plus 594 (1:1,000), and donkey anti-Mouse IgG heavy and light chains–AlexaFluor 647 (1:1,000). Background autofluorescence was then quenched using a 0.1% Sudan Black B solution in 80% ethanol before staining with DAPI. Slides were mounted and then imaged using an Olympus BX61 upright wide-field microscope using Volocity software (version 6.3) with a Hamamatsu ORCA RC camera. Appropriate negative controls without primary antibodies were also imaged using the same exposure time as matching stained sections. Whole-image contrast, brightness and pseudocolouring were adjusted using ImageJ/Fiji (v.2.0.0-rc-69/1.51w) and Adobe Photoshop (version CS6).

RNA in situ hybridization analysis of SARS-CoV-2 infection

RNA in situ hybridization was performed on 10% formalin-fixed, paraffin-embedded 5-µm sections of human lung tissues from LoM using the RNAscope 2.5 HD Reagent Kit according to the manufacturer's instructions (Advanced Cell Diagnostics). In brief, tissue sections

were mounted on Superfrost Plus microscope slides (Fisher Scientific), heated at 60 °C for 1 h, deparaffinized in xylene (2× 5 min) and 100% ethanol (2× 2 min) and air-dried. Tissue sections were then incubated with hydrogen peroxide to block endogenous peroxidases for 10 min at room temperature, followed by epitope retrieval (Advanced Cell Diagnostics) for 30 min in a water bath at 95 °C. Subsequently, tissue sections were immediately washed in double-distilled water then dehydrated in 100% ethanol for 2 min before air-drying. Tissue sections were then incubated with Protease Plus (Advanced Cell Diagnostics) for 30 min at 40 °C in a HybEZ hybridization oven (Advanced Cell Diagnostics). Sections were rinsed 3 times in double-distilled water, and then incubated with a prewarmed target probe designed to hybridize with the spike protein of SARS-CoV-2 (cat. no. 848561, Advanced Cell Diagnostics) for 2 h at 40 °C. Tissue sections were then washed and the signal amplified according to the manufacturer's instructions, and developed using alkaline phosphatase and Fast Red substrate. Tissue sections were counterstained with DAPI, mounted with Prolong Gold (Invitrogen) and imaged on an EVOS M5000 microscope (Invitrogen).

Electron microscopy analysis of SARS-CoV-2 infection

Small pieces of human lung tissue collected from SARS-CoV-2-infected LoM at 2 days after infection were fixed in 4% paraformaldehyde and 2.5% glutaraldehyde in 0.15 M sodium phosphate buffer, pH 7.4, for 2 h at room temperature. The tissues were subsequently transferred to 10% formalin for 7 days. Specimens were washed in 0.1 M sodium cacodylate, pH 7.4, and then post-fixed with 1% cacodylate-buffered osmium tetroxide for 1 h. After washing in 0.05 M sodium cacodylate buffer, pH 7.0, the samples were treated with 1% tannic acid in 0.05 M sodium cacodylate buffer for 30 min to enhance tissue contrast and preserve structure[46]. Tissue pieces were washed in deionized water, dehydrated in ethanol and placed through two exchanges of propylene oxide before infiltration and embedment in PolyBed 812 epoxy resin (Polysciences). Semi-thin (1 µm) sections of tissue blocks were cut and stained with 1% toluidine blue in 1% sodium borate for examination by light microscopy. Ultra-thin (70 nm) sections were cut of selected regions of interest, mounted on 200 mesh copper grids and stained with 4% aqueous uranyl acetate and Reynolds' lead citrate. Grids were observed on a JEOL JEM 1230 transmission electron microscope operating at 80 kV (JEOL USA) and images were acquired with a Gatan Orius SC1000 CCD Digital Camera and Gatan Microscopy Suite software (v.3.0, Gatan). Virus particle sizes were measured in Fiji/Image J (v.2.0.0-rc-69/1.52p).

Processing of human lung tissues from LoM for RNA-sequencing analysis

Human lung tissues from LoM were collected in RNAlater and kept at 4 °C for 24 h before storage at −80 °C until further processing. To isolate RNA, samples stored in RNAlater were thawed and the tissue transferred to a new tube containing 1-mm glass beads and 1 ml Trizol. Tissues were subsequently homogenized using a MagNA Lyser (Roche) for 30 s at 6,000 rpm. Between rounds of homogenization, tissues were incubated on ice for 1 min. Following tissue homogenization, Trizol homogenate was transferred to a new tube and stored at −80 °C.

RNA-sequencing analysis

RNA was extracted from human lung samples from LoM using a Trizol Plus RNA extraction kit (Thermo Fisher), quantified using a Qubit RNA assay kit and checked for quality using a Bioanalyzer RNA600 Nano kit (Agilent). RNA integrity scores were typically 7.0 and greater. One µg of RNA was used to construct libraries for sequencing using a NEBNext Ultra II library prep kit with polyA RNA selection. Barcoded libraries were sequenced on a Novaseq 6000 2×100 bp following manufacturer's instructions (Illumina). Sequence quality was assessed using FASTQC (v.0.11.9). No issues were detected with the data and the quality was typical for RNA extracted from fresh-frozen material. A small amount of index hopping was detected (0.09%), due to the single indices used in the library preparation. Raw reads were mapped to the human, mouse and SARS-CoV-2 reference genomes simultaneously (GRCh38.p13, GRCm38.p6 M25 and NC_045512, respectively) using the BBsplit function in BBmap (v.38.86). This step minimized cross-mapping of reads among genomes. There was a nonsignificant, negative relationship between the amount of viral and human RNA reads ($R^2 = 0.136$). We then mapped and quantified on a transcript and gene model basis using STAR (v.2.7.5a) and Salmon (v.1.2.1)[47,48]. Reads mapping to multiple locations were dropped from analysis. On average, in the human lung tissue samples from LoM, 80 ± 6% (±s.d.) of the reads mapped to human, 19 ± 6% (±s.d.) mapped to mouse and 1 ± 1% (±s.d.) mapped to the SARS-CoV-2 genome. The per cent of virus ranged from 0.05% to 3.4% among infected mice: day-2 mice had the most virus, which is consistent with the infection titres we observed. Samples from naive mice were 95% or more human data.

Statistics and reproducibility

No statistical methods were used to predetermine sample size. No randomization was used to determine allocation of samples or mice to experimental groups and downstream analysis. The investigators were not blinded to group allocation for data collection and analysis. In Fig. 1b, titres for SARS-CoV and MERS-CoV represent two independent experiments, and titres for SARS-CoV-2, WIV1-CoV and SHC014-CoV represent one experiment. Virus titres between SARS-CoV-2-infected LoM analysed 2 days after exposure and days 6 and 14 after exposure (Fig. 1c) were compared with a two-sided Kruskal–Wallis with Dunn's multiple comparisons test; data represent one experiment. Pieces of human lung implants obtained from LoM in Fig. 1c were used for the RNAscope and immunofluorescence analysis shown in Fig. 1d–g, the histological and electron microscopy analyses in Fig. 2, and the RNA-sequencing gene-expression analyses in Fig. 3, Extended Data Fig. 3, Extended Data Tables 3–5, Supplementary Tables 1, 2. The number of independent human lung tissue samples from LoM that were analysed for each parameter is indicated in the figure and table legends. RNA-sequencing data were normalized and investigated for changes in gene expression using DESeq2 package (v.3.1.1) in R (v. 3.6.3)[49]; statistical tests were two-sided. We focused the analysis on the naive controls versus LoM at days 2, 6 and 14 after infection. Wald's tests were performed to contrast each day with naive controls. Because mice were euthanized at each time point, we treated each day independently rather than as a time series. *P* values were adjusted for multiple testing using a false discovery rate using the Benjamini–Hochberg method[50]. Data were analysed both jointly and within each treatment compared to naive controls. Differential expression of outliers was assessed and found to be insignificant in overall effect. Graphs and summary tables were built in R using ggplot; gene-set enrichment was performed using gene-set enrichment analysis and Gene Ontology (GO) analysis (tidyverse 1.3.0, PCATools 1.2.0, Sqldf 0.4-11, na.tools 0.3.1, ggbiplot 0.55, ggplot2 3.3.1 and dplyr 0.8.4). The statistical significance of enrichment scores calculated by gene-set enrichment analysis was determined using an empirical phenotype-based permutation test[51], and *P* values were adjusted for multiple testing using a false discovery rate using the Benjamini–Hochberg method[50]. Specific gene sets of interest were then investigated for patterns of expression across treatment and time using unsupervised clustering of normalized gene-expression counts. GO analysis and visualization were performed with Gorilla (no version)[52]. In Fig. 4, virus titres in LoM dosed with vehicle control or EIDD-2801 were compared with a two-sided Mann–Whitney *U* test (GraphPad Prism v.8.0 or R v.3.5.3). The effect of EIDD-2801 treatment on virus titres (Fig. 4a, b) represents one experiment and the effect of EIDD-2801 prophylaxis (Fig. 4c–e) represents two independent experiments. All independent attempts of repetition were completed with similar results.

Reporting summary

Further information on research design is available in the Nature Research Reporting Summary linked to this paper.

Data availability

Gene-expression data are available at the Gene Expression Omnibus repository (accession number GSE155286). All other data are available from the corresponding author on reasonable request. Publicly available datasets used in this study were: (1) the sequence of the SARS-CoV-2 strain 2019-nCoV/USA-WA1/2020 (GenBank accession number MN985325.1) and (2) human lung tissue gene-expression data profiled by the GTEx project (https://gtexportal.org/home/; data retrieved 20 October 2020 and 3 November 2020). Source data are provided with this paper.

44. Scobey, T. et al. Reverse genetics with a full-length infectious cDNA of the Middle East respiratory syndrome coronavirus. *Proc. Natl Acad. Sci. USA* **110**, 16157–16162 (2013).
45. Yount, B. et al. Reverse genetics with a full-length infectious cDNA of severe acute respiratory syndrome coronavirus. *Proc. Natl Acad. Sci. USA* **100**, 12995–13000 (2003).
46. Simionescu, N. & Simionescu, M. Galloylglucoses of low molecular weight as mordant in electron microscopy. I. Procedure, and evidence for mordanting effect. *J. Cell Biol.* **70**, 608–621 (1976).
47. Dobin, A. et al. STAR: ultrafast universal RNA-seq aligner. *Bioinformatics* **29**, 15–21 (2013).
48. Patro, R., Duggal, G., Love, M. I., Irizarry, R. A. & Kingsford, C. Salmon provides fast and bias-aware quantification of transcript expression. *Nat. Methods* **14**, 417–419 (2017).
49. Love, M. I., Huber, W. & Anders, S. Moderated estimation of fold change and dispersion for RNA-seq data with DESeq2. *Genome Biol.* **15**, 550 (2014).
50. Benjamini, Y. & Hochberg, Y. Controlling the false discovery rate: a practical and powerful approach to multiple testing. *J. R. Stat. Soc.* **57**, 289–300, (1995).
51. Subramanian, A. et al. Gene set enrichment analysis: a knowledge-based approach for interpreting genome-wide expression profiles. *Proc. Natl Acad. Sci. USA* **102**, 15545–15550 (2005).
52. Eden, E., Navon, R., Steinfeld, I., Lipson, D. & Yakhini, Z. GOrilla: a tool for discovery and visualization of enriched GO terms in ranked gene lists. *BMC Bioinformatics* **10**, 48 (2009).

Acknowledgements We thank current and past members of the laboratory of J.V.G. for technical assistance; technicians at the UNC Animal Histopathology and Laboratory Medicine Core and Division of Comparative Medicine; the UNC School of Medicine Bioinformatics and Analytics Research Collaborative (BARC) for providing technical support; and K. Mollan and B. Shook-Sa of the UNC CFAR Biostatistics Core for providing statistical support. This work was supported by funding from National Institutes of Health grants R21AI113736 (R.J.P.), U19AI100625 and R01 AI108197 (R.S.B.), Fast Grants (L.E.G.), R01AI123010 (A.W.), R01AI111899 (J.V.G.), R01AI140799 (J.V.G.) and R01MH108179 (J.V.G.). This project was also supported by the North Carolina Policy Collaboratory at the University of North Carolina at Chapel Hill with funding from the North Carolina Coronavirus Relief Fund established and appropriated by the North Carolina General Assembly. The Microscopy Services Laboratory, Department of Pathology and Laboratory Medicine, is supported in part by P30 CA016086 Cancer Center Support Grant to the UNC Lineberger Comprehensive Cancer Center.

Author contributions A.W., C.E.J., W.Y., M.K. and C.D. constructed LoM. A.W. contributed to experimental design, data interpretation, data presentation and manuscript writing, and coordinated the study and the preparation of the manuscript. L.E.G. performed the virus inoculations, animal necropsies, virus titring and processing of lung tissues for RNA extraction, and contributed to the experimental design, planning, data analysis, data interpretation and manuscript writing. C.E.J. performed immunofluorescence and H&E analyses, W.Y. performed immunohistochemistry and H&E analyses, and M.K. performed the in situ hybridization analysis of LoM human lung tissues. K.H.D., A.S., S.R.L. and K.G. assisted with the in vivo experiments with coronavirus-infected LoM. V.J.M. in conjunction with K.K.W. performed the electron microscopy analysis. G.R.B., A.A.K., M.G.N. and G.P. assisted with the EIDD-2801 experiments. F.B.A. assisted with the pathohistological analysis. H.L., H.M.K., T.Z. and P.O.G. performed the RNA-sequencing analysis. E.P.B. and C.D.J. contributed to the design of RNA-sequencing experiments. R.J.P. assisted with the immunofluorescence analysis, and contributed to experimental design, data interpretation, data presentation and manuscript writing. R.S.B. conceived and designed experiments, and contributed to data interpretation and manuscript writing. J.V.G. conceived, designed and coordinated the study, conceived and designed experiments, and contributed to data interpretation, data presentation and manuscript preparation.

Competing interests G.P., M.G.N., G.R.B. and A.A.K. are employees of Emory and have a financial interest in molnupiravir (EIDD-2801).

Additional information

Supplementary information The online version contains supplementary material available at https://doi.org/10.1038/s41586-021-03312-w.

Correspondence and requests for materials should be addressed to J.V.G.

Peer review information *Nature* thanks the anonymous reviewers for their contribution to the peer review of this work.

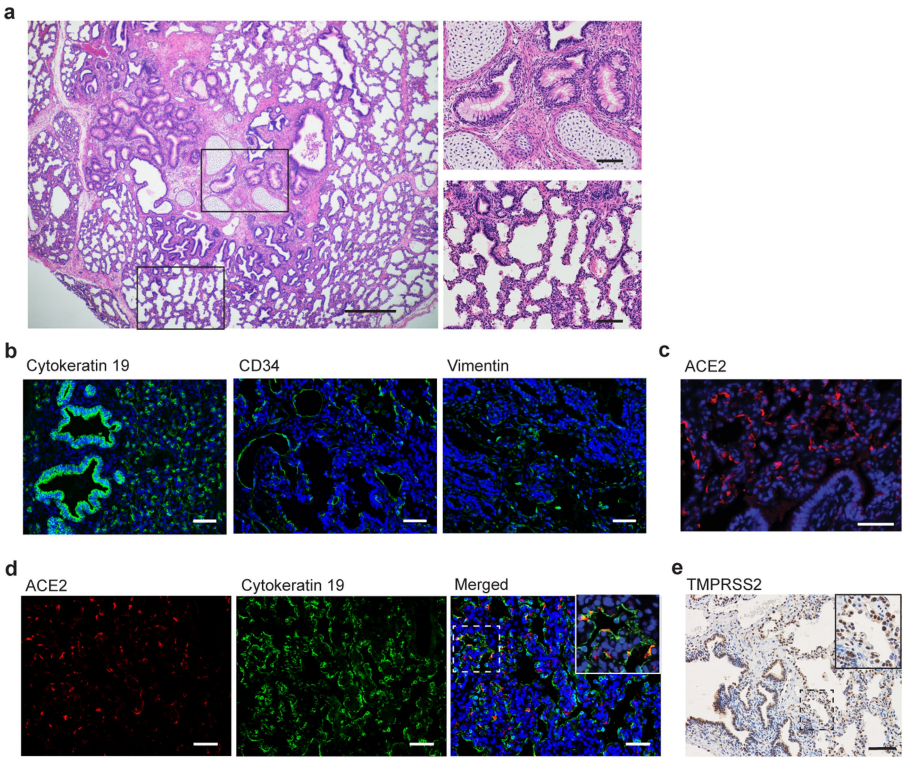

Extended Data Fig. 1 | Human epithelial cells in the human lung tissue of LoM express ACE2. a, H&E staining of the human lung tissue of a naive LoM ($n = 6$). Boxes in the left panel indicate regions that are shown in higher-magnification images in the right panels, of cartilaginous airways (top) and noncartilaginous airways and alveoli (bottom). Scale bars, 500 µm (left), 100 µm (top right, bottom right). **b**, Immunofluorescence staining for human cytokeratin 19 (epithelial cells, green; nuclei, blue), CD34 (endothelial cells, green; nuclei, blue) or vimentin (mesenchymal cells, green; nuclei, blue) ($n = 8$). Scale bars, 50 µm. **c**, Immunofluorescence staining for human ACE2 in the human lung tissue of a naive LoM (positive cells, red; nuclei, blue) ($n = 9$). Scale bar, 50 µm. **d**, Costaining for human ACE2 (positive cells, red) and cytokeratin 19 (positive cells, green) in human lung tissue from naive LoM (nuclei, blue) ($n = 9$). Scale bars, 50 µm. **e**, Immunohistochemical staining for TMPRSS2 in human lung tissue from naive LoM (positive cells, brown) ($n = 6$). Scale bar, 100 µm. *n*, number of biologically independent lung tissues analysed.

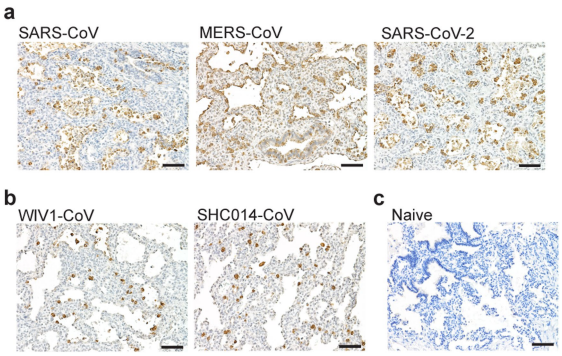

Extended Data Fig. 2 | Viral nucleoprotein in the human lung tissues of LoM infected with recently emerged human coronaviruses and bat coronaviruses. a–**c**, Immunohistochemical staining for virus nucleoprotein in human lung tissue collected from LoM two days after exposure to the recently emerged human coronaviruses SARS-CoV ($n = 4$), MERS-CoV ($n = 5$) or SARS-CoV-2 ($n = 6$) (**a**), LoM two days after exposure to the bat coronaviruses WIV1-CoV or SHC014-CoV ($n = 10$) (**b**) or naive LoM ($n = 6$) (**c**). Positive cells, brown. Scale bars, 100 µm. *n*, number of biologically independent lung tissues analysed.

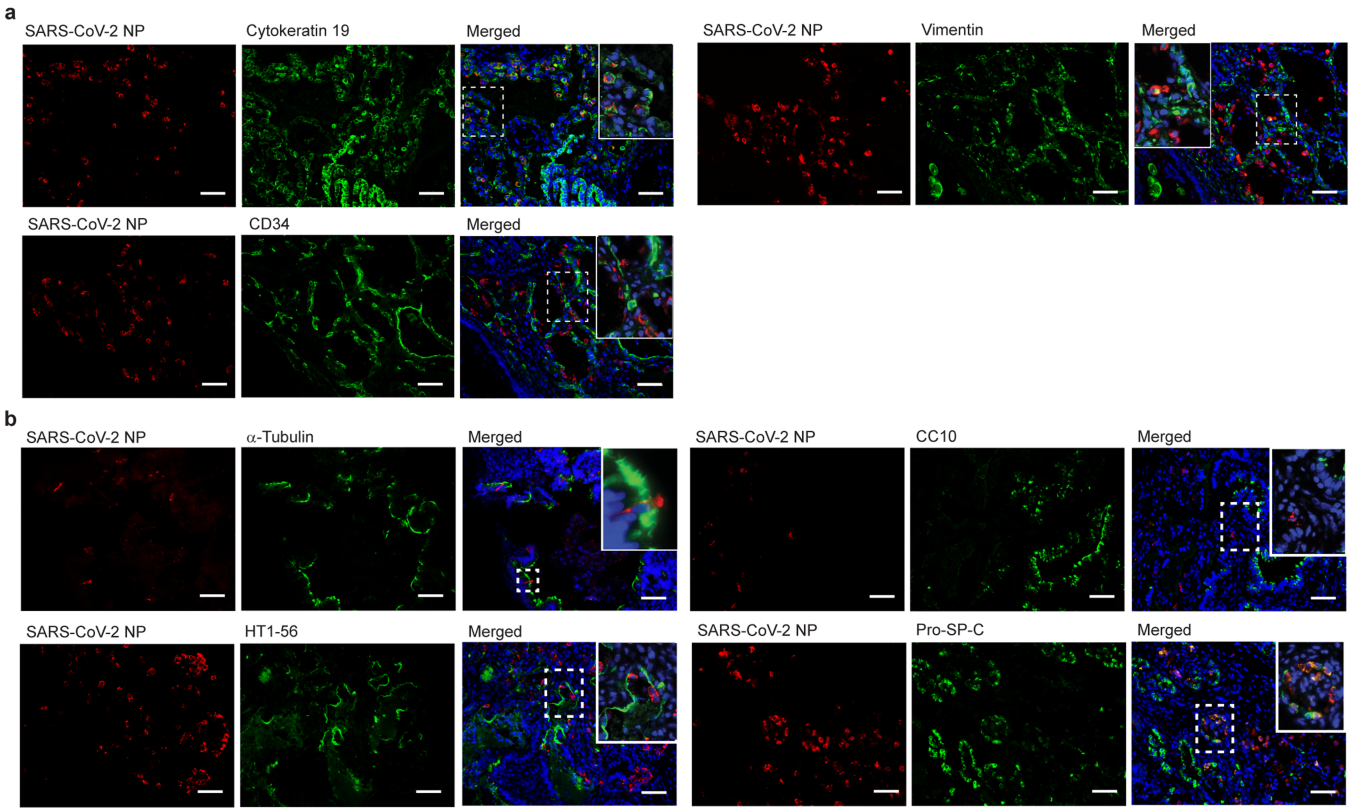

Extended Data Fig. 3 | SARS-CoV-2 infection of human epithelial cell types in the human lung tissue of LoM. a, **b**, Single-colour and merged images of those shown in Fig. 1f, g, depicting costaining of human lung tissue from LoM two days after exposure to SARS-CoV-2 for virus nucleoprotein (red) and cytokeratin 19 (epithelial cells, green) ($n = 6$), CD34 (endothelial cells, green) ($n = 4$) or vimentin (mesenchymal cells, green) ($n = 4$) (**a**) or acetylated α-tubulin IV (ciliated cells, green) ($n = 6$), CC10 (club cells, green) ($n = 6$), HT1-56 (alveolar type-1 pneumocytes, green) ($n = 6$) or pro-SP-C (alveolar type-2 pneumocytes, green) ($n = 3$) (**b**). Nuclei, blue. Scale bars, 50 µm. *n*, number of biologically independent lung tissues analysed.

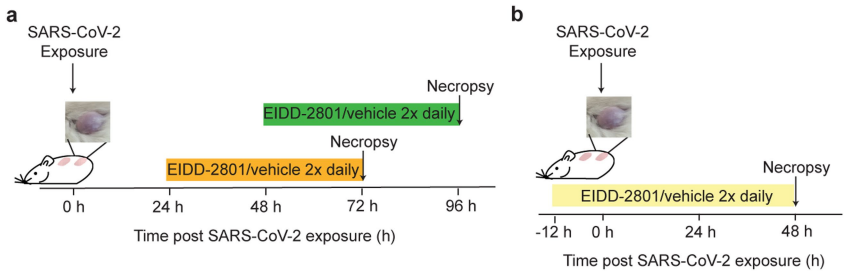

Extended Data Fig. 4 | Experimental design for the evaluation of EIDD-2801 as a treatment or pre-exposure prophylaxis for infection with SARS-CoV-2. **a**, Experimental design for treatment. LoM were orally administered EIDD-2801 or vehicle at 24 h or 48 h after exposure to SARS-CoV-2, and every 12 h thereafter. Virus titres were measured two days after the initiation of treatment. **b**, Experimental design for pre-exposure prophylaxis. LoM were orally administered EIDD-2801 or vehicle control 12 h before exposure to SARS-CoV-2, and every 12 h thereafter. Virus titres in human lung tissues were measured two days after exposure.

Extended Data Table 1 | Description of LoM used for the analysis of human and bat coronavirus replication

Group	Mouse	Sex	Human donor	Weeks post-surgery
SARS-CoV	1	F	O32	10
	2	F	O32	10
	3	M	U32	9
	4	M	U32	9
	5	F	I33	14
	6	F	L33	10
	7	F	L33	10
	8	F	L33	10
MERS-CoV	9	M	D33	9
	10	M	D33	9
	11	M	F33	9
	12	M	F33	9
	13	F	I33	14
	14	F	L33	10
	15	F	L33	10
	16	F	L33	10
SARS-CoV-2	17	F	O32	19
	18	F	O32	19
	19	M	D33	14
	20	M	F33	14
WIV-CoV	21	M	F33	20
	22	M	F33	20
	23	M	F33	20
SHC014-CoV	24	M	F33	20
	25	M	F33	20
	26	M	F33	20

Extended Data Table 2 | Description of LoM used for the analysis of SARS-CoV-2 replication and pathogenesis over time

Group	Mouse	Sex	Human donor	Weeks post-surgery
Day 2	27	F	A31	59
	28	F	A31	59
	29	F	F32	25
	30	F	I32	19
Day 6	31	F	R30	74
	32	F	A31	59
	33	F	I32	19
	34	F	F32	25
	35	F	F32	25
Day 14	36	F	A31	59
	37	F	I32	19
	38	F	R30	74
	39	F	F32	25
	40	F	F32	25

Extended Data Table 3 | Abundance of viral transcripts detected in LoM infected with SARS-CoV-2

Group	Mouse	Sex	Human donor	Weeks post-surgery	%Viral transcripts
Day 2	1	F	A31	59	0.55301%
	41	F	I32	19	3.55979%
Day 6	31	F	R30	74	1.01818%
	32	F	A31	59	0.46368%
	33	F	I32	19	1.38159%
Day 14	37	F	I32	19	0.69389%
	39	F	F32	25	0.05856%
	42	F	A31	59	0.18557%
Naive	43	F	A31	59	N/A
	44	F	I32	19	N/A
	45	F	I32	19	N/A
	46	F	I32	19	N/A

The per cent viral transcripts of total transcripts sequenced from SARS-CoV-2-infected (n = 8) and naive (n = 4) LoM used for RNA-sequencing analysis is shown. Using a linear model, there was no effect of human donor on viral transcript abundance (lm() in R: estimate −0.012, P = 0.103). n, number of biologically independent lung tissues analysed. N/A, not applicable.

Extended Data Table 4 | Abundance of human *ACE2* and *TMPRSS2* transcripts detected in LoM infected with SARS-CoV-2

Group	Mouse	Human donor	GAPDH (TPM)	ACE2 (TPM)	TMPRSS2 (TPM)
Day 2	1	A31	517.41	1.79	33.54
	41	I32	432.19	4.63	41.96
Day 6	31	R30	654.63	2.67	78.64
	32	A31	784.39	0.73	21.62
	33	I32	481.94	1.56	41.07
Day 14	37	I32	419.55	2.02	38.94
	39	F32	492.57	1.90	61.95
	42	A31	351.54	1.54	43.50
Naive	43	A31	2384.62	0.19	15.35
	44	I32	363.42	0.82	38.95
	45	I32	359.21	0.67	38.19
	46	I32	339.77	0.89	32.93

The abundance of human *GAPDH*, *ACE2* and *TMPRSS2* transcripts sequenced in human lung tissue collected from naive ($n = 4$) and SARS-CoV-2-infected ($n = 8$) LoM is shown. The median *ACE2* and *TMPRSS2* expression in human lung tissue of naive mice was 0.75 and 35.6 TPM, respectively, which is comparable to the median expression of *ACE2* (1.01 TPM) and *TMPRSS2* (43.2 TPM) observed in human lung tissue profiled by the GTEx project (https://gtexportal.org/home/; data retrieved 20 October 2020 and 3 November 2020). No effect of human donor on *ACE2* expression ($F = 2.06259641$; $P = 0.1756$ via two-sided analysis of variance) was observed. Approximately the same amount of variation was observed within a human donor (mean variance within donors = 4.82) as across all donors (variance = 4.47). *n*, number of biologically independent lung tissues analysed.

Extended Data Table 5 | Human interferon and cytokine genes upregulated during infection with SARS-CoV-2

		Naive	Day 2			Day 6			Day 14		
	Gene	TPM	TPM	Log2FC	p-value	TPM	Log2FC	p-value	TPM	Log2FC	p-value
Interferon genes	IFNB1	0.009721	12.89298	10.8264	N/A	0.56133	5.919101	0.000104	1.261203	6.816893	8.95E-07
	ISG15	29.11072	3529.547	7.5504869	N/A	1057.532	5.559945	N/A	680.674	4.441103	4.38E-18
	OASL	0.575651	117.7447	7.460388	N/A	24.14577	5.349643	4.82E-21	19.32386	4.837053	3.70E-40
	MX2	2.446529	207.3412	7.1723067	N/A	54.58907	4.403233	4.35E-16	73.59163	4.793127	3.89E-23
	IFITM1	75.8737	1380.718	6.8014838	N/A	841.8657	3.67271	0.027036	752.1089	3.183608	0.056391
	MX1	10.01414	1098.343	6.6205208	N/A	282.2782	4.583841	1.03E-35	320.7999	4.690323	9.58E-119
	OAS1	5.455972	427.8919	6.3944922	N/A	109.1991	4.097581	4.61E-13	128.1803	4.407948	4.03E-33
	IFIT2	5.663018	327.3042	5.8248817	N/A	40.06805	2.678602	1.04E-12	51.76333	3.021741	3.65E-11
	IFIT3	9.293879	323.3581	5.5590143	N/A	77.21678	2.973115	3.24E-09	90.51719	3.168749	9.62E-11
	OAS3	4.160792	118.0739	5.1575147	N/A	27.98228	2.619502	5.04E-13	32.44652	3.006743	1.07E-25
Cytokine genes	CXCL10	1.334587	784.985	9.4483016	N/A	51.89486	5.060381	3.36E-08	104.6776	6.211797	2.26E-28
	CXCL11	0.368657	170.7106	9.0255049	N/A	13.74948	5.100041	1.73E-13	28.97534	6.20993	4.12E-32
	CCL7	0.110614	2.114279	8.1032148	N/A	0.256785	0.939467	0.826964	4.136358	5.155454	0.0337375
	CXCL9	0.31541	20.86055	6.5863786	N/A	13.58781	5.142114	N/A	51.63909	7.324334	N/A
	CXCL8	8.329686	33.28712	6.3670255	N/A	88.08344	2.850492	N/A	6.213093	-0.60592	N/A
	CXCL2	6.093913	114.8106	5.9559545	N/A	51.26291	2.979872	0.018944	24.8723	2.026886	0.1230292
	CCL8	0.872448	31.60003	5.7008898	N/A	3.819344	2.129537	0.000334	11.39742	3.657159	2.66E-05
	CCL5	0.708453	12.48674	5.5750578	N/A	4.494502	2.620838	0.029157	19.43851	4.710446	7.17E-05
	IL6	5.42304	12.23683	5.0378314	N/A	27.2112	1.542807	N/A	3.889728	-0.96496	N/A
	IL27	0.02044	0.802539	4.5555662	N/A	0.144501	2.957134	0.168998	0.166259	2.840334	0.0473019
	CXCL3	1.665821	17.51558	4.0723405	N/A	7.100009	2.13156	0.03234	6.128888	1.776734	0.0077687
	IL17C	0.040803	0.246641	3.4322656	N/A	0.069498	1.136046	0.651685	0.079223	0.819111	0.815461
	TNF	0.252698	0.776601	2.6658632	N/A	0.370601	0.713121	0.693592	1.728727	2.737404	N/A

Shown is the $\log_2$-transformed fold change (Log2FC) in TPM detected in human lung tissues from LoM at 2 (n = 2), 6 (n = 3) and 14 (n = 3) days after exposure to SARS-CoV-2, compared to naive control mice (n = 4). P values were calculated in DESeq2 using a two-sided Wald's test and adjusted for multiple testing using a false discovery rate. For samples marked not applicable (N/A), DESeq2 could not calculate a P value owing to sample size or the variance between samples. n, number of biologically independent lung tissues analysed.

Extended Data Table 6 | Description of LoM used to evaluate the efficacy of EIDD-2801 in the treatment of SARS-CoV-2 infection or as pre-exposure prophylaxis

Group	Mouse	Sex	Human donor	Weeks post-surgery
Vehicle pre-exposure prophylaxis	47	M	F33	15
	48	M	F33	15
	49	F	L33	11
	50	F	L33	11
	51	M	T33	13
	52	M	T33	13
	53	M	T33	13
	54	M	T33	13
EIDD-2801 pre-exposure prophylaxis	55	M	F33	15
	56	M	F33	15
	57	F	L33	11
	58	F	L33	11
	59	M	T33	13
	60	M	T33	13
	61	M	T33	13
	62	M	T33	13
Vehicle 24h treatment	63	F	C34	16
	64	F	C34	16
	65	F	C34	16
	66	F	C34	16
EIDD-2801 24h treatment	67	F	C34	16
	68	F	C34	16
	69	F	C34	16
	70	F	C34	16
Vehicle 48h treatment	71	F	C34	16
	72	F	C34	16
	73	F	C34	16
	74	F	C34	16
EIDD-2801 48h treatment	75	F	C34	16
	76	F	C34	16
	77	F	C34	16
	78	F	C34	16

nature research

Corresponding author(s): J. Victor Garcia

Last updated by author(s): Jan 7, 2021

Reporting Summary

Nature Research wishes to improve the reproducibility of the work that we publish. This form provides structure for consistency and transparency in reporting. For further information on Nature Research policies, see our Editorial Policies and the Editorial Policy Checklist.

Statistics

For all statistical analyses, confirm that the following items are present in the figure legend, table legend, main text, or Methods section.

n/a	Confirmed	
☐	☒	The exact sample size (*n*) for each experimental group/condition, given as a discrete number and unit of measurement
☐	☒	A statement on whether measurements were taken from distinct samples or whether the same sample was measured repeatedly
☐	☒	The statistical test(s) used AND whether they are one- or two-sided *Only common tests should be described solely by name; describe more complex techniques in the Methods section.*
☒	☐	A description of all covariates tested
☐	☒	A description of any assumptions or corrections, such as tests of normality and adjustment for multiple comparisons
☐	☒	A full description of the statistical parameters including central tendency (e.g. means) or other basic estimates (e.g. regression coefficient) AND variation (e.g. standard deviation) or associated estimates of uncertainty (e.g. confidence intervals)
☐	☒	For null hypothesis testing, the test statistic (e.g. *F*, *t*, *r*) with confidence intervals, effect sizes, degrees of freedom and *P* value noted *Give P values as exact values whenever suitable.*
☒	☐	For Bayesian analysis, information on the choice of priors and Markov chain Monte Carlo settings
☒	☐	For hierarchical and complex designs, identification of the appropriate level for tests and full reporting of outcomes
☒	☐	Estimates of effect sizes (e.g. Cohen's *d*, Pearson's *r*), indicating how they were calculated

Our web collection on statistics for biologists contains articles on many of the points above.

Software and code

Policy information about availability of computer code

Data collection	Nikon Elements BR software (version 4.30.01), Volocity software (version 6.3), Gatan Microscopy Suite software (version 3.0)
Data analysis	ImageJ/Fiji (version 2.0-rc-69/1.51w), Adobe Photoshop (version C S6), FASTQC (version 0.11.9), BBmap (version 38.86), STAR (version 2.7.5a), Salmon (version 1.2.1), DESeq2 (version 3.1.1), R (version 3.5.3 or 3.6.3), GOrilla (no version), tidyverse (version 1.3.0), PCATools (version 1.2.0), Sqldf (version 0.4-11), na.tools (version 0.3.1), ggbiplot (version 0.55), ggplot2 (version 3.3.1), dplyr (version 0.8.4), Graphpad Prism (version 8.0.0)

For manuscripts utilizing custom algorithms or software that are central to the research but not yet described in published literature, software must be made available to editors and reviewers. We strongly encourage code deposition in a community repository (e.g. GitHub). See the Nature Research guidelines for submitting code & software for further information.

Data

Policy information about availability of data

All manuscripts must include a data availability statement. This statement should provide the following information, where applicable:

- Accession codes, unique identifiers, or web links for publicly available datasets
- A list of figures that have associated raw data
- A description of any restrictions on data availability

Gene-expression data are available at the Gene Expression Omnibus (GEO) repository (accession: GSE155286). Source data is provided for Fig. 1b,c and Fig. 4a-d. All other data is available from corresponding authors on reasonable request. Publicly available data sets used in this study: 1) sequence of the SARS-CoV-2 strain 2019-nCoV/USA-WA1/2020 (GenBank accession: MN985325.1) and 2) human lung tissue gene expression data profiled by the GTEx project (https://gtexportal.org/home/; data retrieved 10/20/2020 and 11/3/2020).

Field-specific reporting

Please select the one below that is the best fit for your research. If you are not sure, read the appropriate sections before making your selection.

☒ Life sciences ☐ Behavioural & social sciences ☐ Ecological, evolutionary & environmental sciences

For a reference copy of the document with all sections, see nature.com/documents/nr-reporting-summary-flat.pdf

Life sciences study design

All studies must disclose on these points even when the disclosure is negative.

Sample size	No statistical methods were used to predetermine sample size. To aid statistical analysis, at least 3 samples were used for each group, unless otherwise noted. At least three animals were utilized for each virus and time point. The number of animals per group was also influenced by the number different analyses performed for each experiment (e.g. virus titer, immunofluorescence/immunohistochemistry, electron microscopy, and/or RNA-sequencing) and so that at least three animals per group were represented for each downstream analysis unless otherwise noted.
Data exclusions	No data was excluded from analysis.
Replication	For the analysis of coronavirus replication in LoM, SARS-CoV and MERS-CoV infections represented 4 human donor cohorts. For the analysis of SARS-CoV-2 replication over time, 4 human donor cohorts were represented. For the analysis of the protective efficacy of EIDD-2801, 3 human donor cohorts were represented and the experiment performed twice. All attempts at replication were successful.
Randomization	No randomization was used to determine how samples/animals were allocated to experimental groups or processed. Mice were allocated to groups based on their implant sizes and their donor cohort to keep experimental groups relatively equivalent with these covariates. Whole implants or pieces of implants (depending on size) from each animal were allocated for analysis by virus titer, immunofluorescence/ immunohistochemistry, electron microscopy, and/or RNA-sequencing so that at least three animals per group were represented (with the exception of the day 2 RNA-seq analysis) and human donor cohorts were represented as equivalently.
Blinding	The investigators were not blinded to group allocation for data collection and analysis. For virus titer measurements, the infecting strain determines what type of cells are used for plaque assays. For example, MERS-CoV is titered on Vero CCL81 cells while SARS-CoV, SARS-CoV-2, WIV-1, and SHC014 are titered using Vero E6 cells. For the RNA-seq analysis, viral and human gene transcripts were analyzed from the same sample. For RNAscope, immunoflourescense, and immunohistochemistry the infecting strain also determines which RNA probe or antibody is used to analyze tissues sections for detection of virus infected cells. H/E staining was often done in parallel. Due to COVID-19 restrictions, personnel who performed histological assays also performed data analysis. For electron microscopy analysis, only SARS-CoV-2 infected human lung tissues were analyzed. Personnel at the UNC Animal Histopathology and Clinical Chemistry Core who performed MSB staining were not privy to group allocations.

Reporting for specific materials, systems and methods

We require information from authors about some types of materials, experimental systems and methods used in many studies. Here, indicate whether each material, system or method listed is relevant to your study. If you are not sure if a list item applies to your research, read the appropriate section before selecting a response.

Materials & experimental systems

n/a	Involved in the study
☐	☒ Antibodies
☐	☒ Eukaryotic cell lines
☒	☐ Palaeontology and archaeology
☐	☒ Animals and other organisms
☒	☐ Human research participants
☒	☐ Clinical data
☒	☐ Dual use research of concern

Methods

n/a	Involved in the study
☒	☐ ChIP-seq
☒	☐ Flow cytometry
☒	☐ MRI-based neuroimaging

Antibodies

Antibodies used	anti-ACE2; clone: Polyclonal IgG; dilution 1:200 dilution; supplier: R&D systems; catalog: AF933 ; lot: HOK0320032; application: IF; https://www.rndsystems.com/products/human-hamster-ace-2-antibody_af933 anti-Acetylated alpha-tubulin; clone: 6-11B-1; dilution: 1:500; supplier: Zymed; catalog: 32-2700; lot: 60806682R; application: IF; https://www.thermofisher.com/antibody/product/Acetyl-alpha-Tubulin-Lys40-Antibody-clone-6-11B-1-Monoclonal/32-2700 anti-CC10; clone: E-11; dilution: 1:500; supplier: Santa Cruz Biotech; catalog: SC-365992; lots: B2219, K10106; application: IF; https://www.scbt.com/p/cc10-antibody-e-11?requestFrom=search

anti-CD34; clone: QBEnd10; dilution: 1:100; supplier: Dako; catalog: M7165; lot: 20011397; application: IF; https://www.agilent.com/store/productDetail.jsp?catalogId=M716501-2

anti-Cytokeratin19; clone: A53-B/A2; dilution: 1:250; supplier: Abcam; catalog: ab7754; lot: GR3226692-4; application: IF; https://www.abcam.com/cytokeratin-19-antibody-a53-ba2-cytoskeleton-marker-ab7754.html

anti-HT1-56; dilution: 1:150; supplier: Terrace Biotech; catalog: TB-29; lot: AHT1-56 HM29; application: IF; https://www.terracebiotech.com/antibodies

anti-MERS nucleocapsid; clone: Polyclonal; dilution: 1:2,000; supplier: LS Bio; catalog: LS-C483529; lot: 127989; application: IHC; https://www.lsbio.com/antibodies/mers-cov-nucleoprotein-antibody-elisa-wb-western-ls-c483529/496447

anti-Pro-SP-C; clone: Polyclonal; dilution: 1:500; supplier: Seven Hills; catalog: WRAB9337; lots: 458, 0206A; application: IF; https://www.sevenhillsbioreagents.com/products/anti-pro-sp-c-rabbit-n-terminal?_pos=1&_sid=51b111a78&_ss=r

anti-SARS nucleocapsid; clone: Polyclonal IgG; dilution: 1:500; supplier: Invitrogen; catalog: PA1-41098, lot: VC2962205; application: IF and IHC; https://www.thermofisher.com/antibody/product/SARS-Coronavirus-Nucleocapsid-Antibody-Polyclonal/PA1-41098

anti-SARS nucleocapsid; dilution: 1:1,000; supplier: Baric Laboratory; application: IF

anti-TMPRSS2; clone: Polyclonal Ig; dilution: 1:100; supplier: MyBioSource; catalog: MBS9215011, lot:SH200730AC; application: IHC; https://www.mybiosource.com/polyclonal-human-antibody/tmprss2/9215011

anti-Vimentin; clone: V9; dilution: 1:100; supplier: Abcam; catalog: ab8069; lot: GR3226692-4; application: IF; https://www.abcam.com/vimentin-antibody-v9-cytoskeleton-marker-ab8069.html

anti-Mouse IgG heavy and light chains-AlexaFluor 488; clone: donkey polyclonal IgG; dilution: 1:1,000; supplier: Invitrogen; catalog: A21202; lot: 2147618; application: IF; https://www.thermofisher.com/antibody/product/Donkey-anti-Mouse-IgG-H-L-Highly-Cross-Adsorbed-Secondary-Antibody-Polyclonal/A-21202

anti-Rabbit IgG heavy and light chains-AlexaFluor 488; clone: donkey polyclonal IgG; dilution: 1:1,000; supplier: Invitrogen; catalog: A21206; lot: 2156521; application: IF; https://www.thermofisher.com/antibody/product/Donkey-anti-Rabbit-IgG-H-L-Highly-Cross-Adsorbed-Secondary-Antibody-Polyclonal/A-21206

anti-Goat IgG heavy and light chains-AlexaFluor 594; clone: donkey Polyclonal IgG; dilution: 1:1,000; supplier: Invitrogen; catalog: A11058; supplier: 2045324; application: IF; https://www.thermofisher.com/antibody/product/Donkey-anti-Goat-IgG-H-L-Cross-Adsorbed-Secondary-Antibody-Polyclonal/A-11058

anti-Mouse IgG heavy and light chains-AlexaFluor Plus 594; clone: donkey Polyclonal IgG; dilution: 1:1,000; supplier: Invitrogen A32744; catalog: UL292347; application: IF; https://www.thermofisher.com/antibody/product/Donkey-anti-Mouse-IgG-H-L-Highly-Cross-Adsorbed-Secondary-Antibody-Polyclonal/A32744

anti-Rabbit IgG heavy and light chains-AlexaFluor Plus 594; clone: donkey Polyclonal IgG; dilution: 1:1,000; supplier: Invitrogen A32754; catalog: VB292347; application: IF; https://www.thermofisher.com/antibody/product/Donkey-anti-Rabbit-IgG-H-L-Highly-Cross-Adsorbed-Secondary-Antibody-Polyclonal/A32754

anti-Mouse IgG heavy and light chains-AlexaFluor 647; clone donkey Polyclonal IgG; dilution: 1:1,000; supplier: Invitrogen; catalog: A31571; lot: 2045337; application: IF; https://www.thermofisher.com/antibody/product/Donkey-anti-Mouse-IgG-H-L-Highly-Cross-Adsorbed-Secondary-Antibody-Polyclonal/A-31571

Validation

The specificity of the antibodies purchased from commercial sources (R&D Systems, Zymed, Santa Cruz Biotech, Dako, Abcam, Terrace Biotech, LS Bio, Seven Hills, and Invitrogen) were validated by the manufacturer as noted on their website (links provided above for each antibody). anti-SARS nucleoprotein mouse serum was produced by the Baric laboratory and validated for immunohistochemistry and immunofluorescence using COVID-19 autopsy lung sections and SARS-CoV-2 infected human airway epithelial cell cultures (https://www.cell.com/cell/pdf/S0092-8674%2820%2930675-9.pdf).

Eukaryotic cell lines

Policy information about cell lines

Cell line source(s)	Vero E6 cells and Vero CCL81 cells were purchased from ATCC
Authentication	Cell lines were authenticated by morphological identification and virus susceptibility profiles.
Mycoplasma contamination	Cell lines were tested negative for mycoplasma by the supplier.
Commonly misidentified lines (See ICLAC register)	No commonly misidentified cell lines were used

Animals and other organisms

Policy information about studies involving animals; ARRIVE guidelines recommended for reporting animal research

Laboratory animals	Lung-only mice (LoM) were constructed using 12-21 week old male and female NOD.Cg-Prkdcscid Il2rgtm1Wjl/SzJ mice (NSG; The Jackson Laboratory, Bar Harbor, ME) mice. Mice were housed in a temperature (20-23°C) and humidity (30-70%) controlled room on a 12 hour light/12 hour dark schedule.
Wild animals	The study did not involve wild animals.
Field-collected samples	The study did not involve field collected samples.
Ethics oversight	Animal studies were carried out according to protocols approved by the Institutional Use and Care Committee at UNC-Chapel Hill and in adherence to the NIH Guide for the Care and Use of Laboratory Animals.

Note that full information on the approval of the study protocol must also be provided in the manuscript.